ORGANIZED BY |

Multi-source remote sensing for urban infrastructure health monitoring

Instructed by: Liu Xianglei, Wang Runjie

Beijing University of Civil Engineering and Architecture, China

A tutorial on ISPRS Geo-Spatial Week, GSW 2025

6th April, 2025

Catalogue

1.1 Research background

Aging urban infrastructure collapses due to poor monitoring are common globally.

2021.
United States of America
A 12-story residential building collapsed in Florida.

2025.
Belgium
A highway bridge collapsed during construction.

2023.
Norway
The collapse of the Randklev Bridge span.

2024.
China
The sudden collapse of a residential building in Tongling.

1.1 Research background

China is the world's leading infrastructure nation, and its urban infrastructure monitoring is in high demand.

No.	Bridge Name	Length (km)	Country	Completion Year
1	Hong Kong-Zhuhai-Macao Bridge	50	China	2018
2	Hangzhou Bay Bridge	36	China	2008
3	Qingdao Haiwan Bridge	35.4	China	2011
4	Donghai Bridge	32.5	China	2005
5	Dalian Bay Cross-sea Project	27	China	2023
6	King Fahd Causeway	25	Bahrain	1986
7	Zhoushan Archipelago Bridge	25	China	2009
8	Shenzhong Corridor Project	24	China	2024
9	Chesapeake Bay Bridge	19.7	USA	1964
10	Great Belt Bridge	17.5	Denmark	1997

No.	Building Name	Height (m)	Country	Completion Year
1	Burj Khalifa	828	UAE	2010
2	Merdeka 118	678.9	Malaysia	2022
3	Shanghai Tower	632	China	2015
4	Abraj Al-Bait Clock Tower	601	Saudi Arabia	2012
5	Ping An Finance Centre	599	China	2017
6	Lotte World Tower	555	South Korea	2016
7	One World Trade Center	541.3	USA	2014
8	Guangzhou CTF Finance Centre	530	China	2016
9	Tianjin CTF Finance Centre	530	China	2019
10	CITIC Tower	528	China	2018

China has 7 out of the top 10 cross-sea bridges globally.

China has 5 out of the top 10 tallest buildings globally.

1.1 Research background

The demand for urban infrastructure monitoring is increasing in various countries.

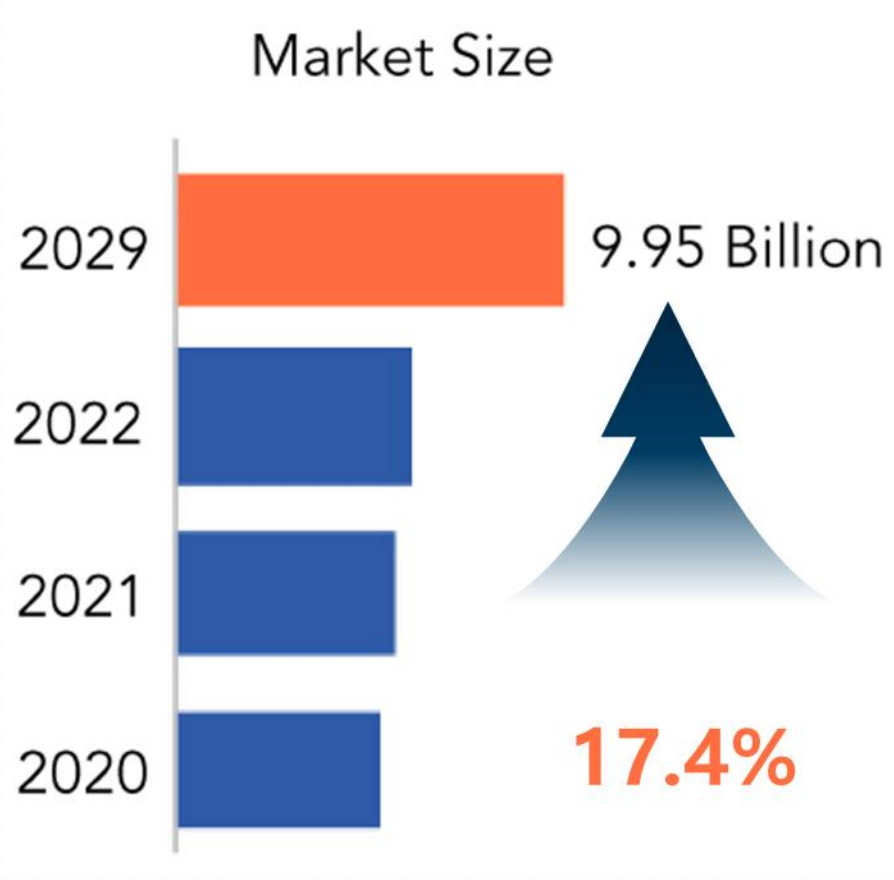

Demand for field of view continues to increase

CHINA

- Establishing Urban Infrastructure GIS

America

- Developing the MIDAS System

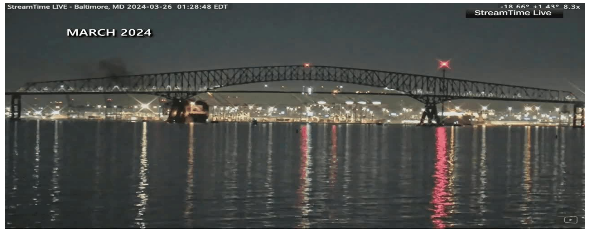

European Union

- Supported by CEF funds

Japan

- Infrastructure Monitoring System

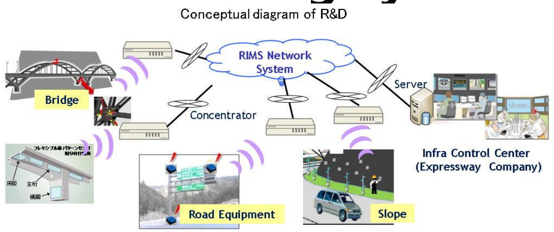

Countries increase attention in infrastructure monitoring

1.1 Research background

Traditional monitoring techniques have problems at all stages of monitoring.

Traditional monitoring technology

Bridge health monitoring system

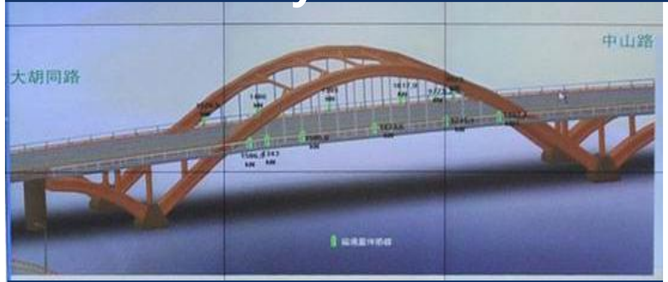

Visual inspection + geodetic survey

Bridge inspection vehicle

Leveling

Manual detection

total station

Stage1: Comprehensive Monitoring and Screening of Damaged Buildings → Lack of efficiency

Stage2: Rapid Detection of Potential Damage Areas → Lack of precision

Stage3: High-Precision Detection of Damage Locations → Lack of credibility

Stage4: Pre-Construction Stability Monitoring → Lack of attention to structural

Overcoming the limitations of traditional measurement techniques is necessary

1.2 Remote Sensing

Remote sensing is a technology that uses sensors to acquire and analyze information about the Earth's surface or other objects from a distance, without direct contact.

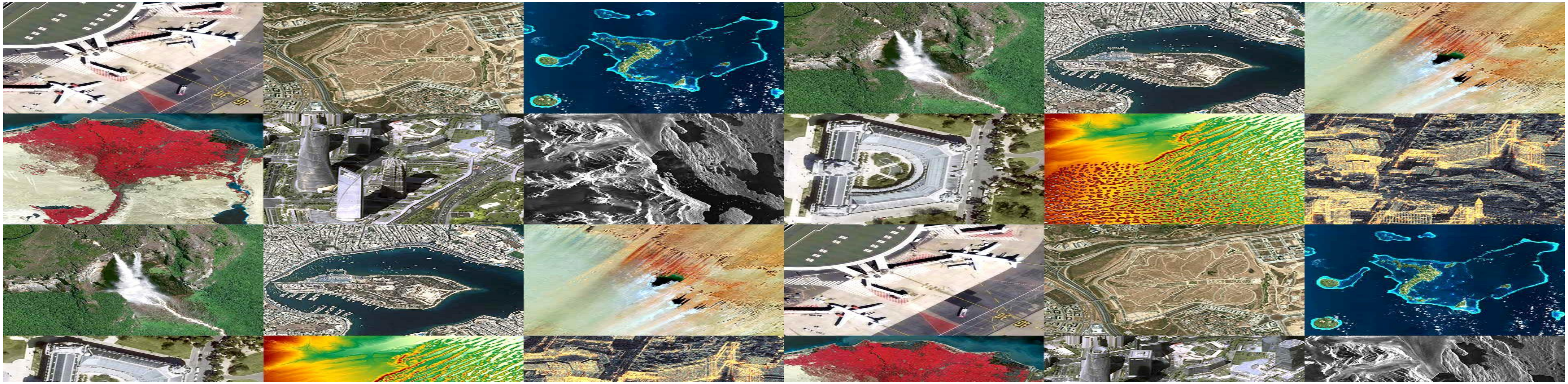

More efficient

It supports large-scale screening.

Higher precision

It can achieve more precise detection.

Higher credibility

Its detection results are more reliable.

Non-contact

It won't cause any damage to the buildings.

1.2 Remote Sensing

Completed buildings are typical urban infrastructure that requires remote sensing technologies capable of wide-area monitoring and high mobility.

Remote sensing measurements

Interferometric synthetic aperture radar (InSAR)

Terrestrial Laser Scanning (TLS)

Ground-based synthetic aperture radar (GB-SAR)

Typical urban buildings

Residential Buildings

Large Shopping Malls

Sports Stadiums

Historic Pagodas and Buildings

School Teaching Buildings

Office Buildings

Bridges

Overpass

Metro Stations

Airport Terminals

Transmission Line

Underground Pipeline

1.2 Remote Sensing

Uncompleted buildings, often unique urban infrastructure, require remote sensing technologies like high-speed cameras that excel at capturing fine detail changes.

Remote sensing measurements

High-speed cameras

Shaking table

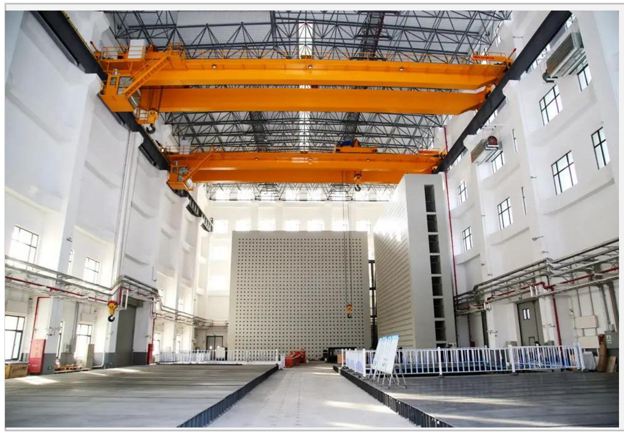

Domestic Largest Total Capacity
BUCEA Multi-functional Seismic Testing Platform

Distinctive urban buildings

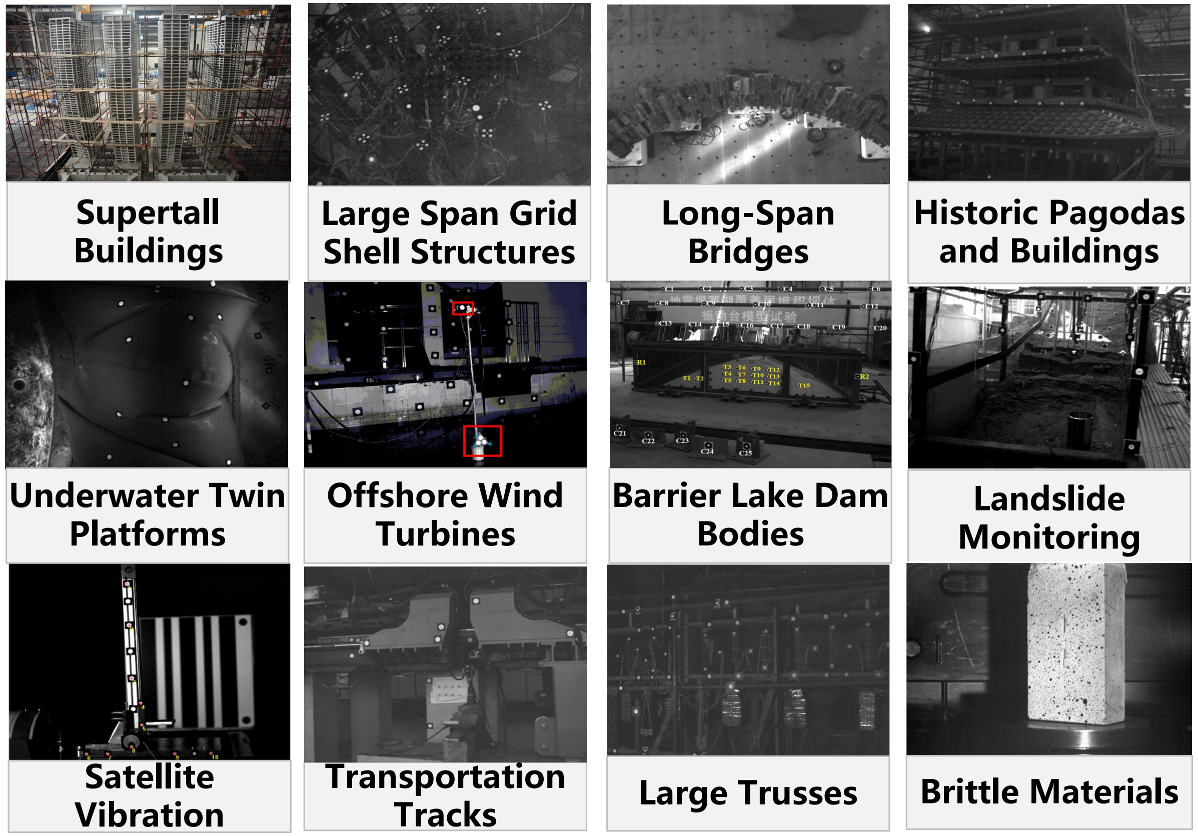

BUCEA: Beijing University of Civil Engineering and Architecture

1.2 Remote Sensing

BUCEA currently has China's largest total capacity multifunctional shaking table laboratory. Four shaking tables are being built, each capable of simulating three-directional, six-degree-of-freedom seismic vibrations.

Shaking table

Typical experiment

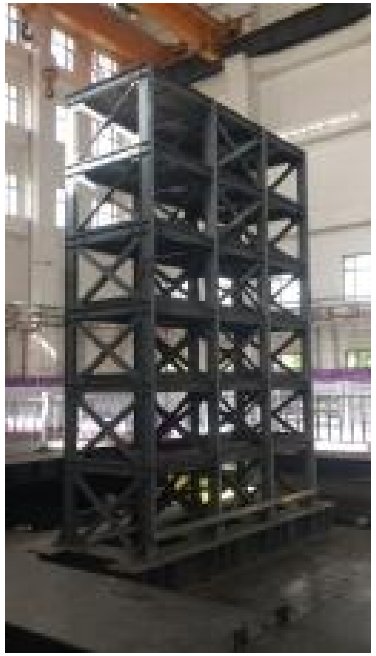

Collaborative research or test needs is warmly welcome from potential partners

BUCEA: Beijing University of Civil Engineering and Architecture

1.3 Multi-source Remote Sensing

Each remote sensing technique has its own advantages and disadvantages

InSAR

Advantages:
- Large monitoring range
- Long monitoring time

Disadvantages:
- Low resolution
- Poor flexibility

TLS

Advantages:
- High resolution
- High flexibility

Disadvantages:
- Limited penetration
- Highly affected by weather

GB-SAR

Advantages:
- High dynamic
- Not affected by weather

Disadvantages:
- Low frame rate
- Poor visibility

High-speed camera

Advantages:
- High frame rate
- High visibility

Disadvantages:
- High price
- Trouble setting up

Single remote sensing technology is not sufficient for urban infrastructure monitoring.

1.3 Multi-source Remote Sensing

Multi-source remote sensing overcomes single-source limitations for comprehensive urban infrastructure monitoring.

Multi-source remote sensing for urban health monitoring

Operation and Maintenance Stage

InSAR

Comprehensive Damage Monitoring

TLS

Quick Potential Damage Detection

GB-SAR

High-Precision Damage Location Detection

Pre-Construction Stability Monitoring Stage

Shaking Tables

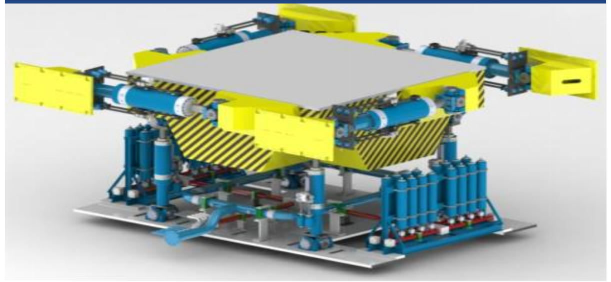

Build a model for shaking tables

Shaking Experiment

Vibration simulation on the shaking table

High-speed camera

Pre-Construction Stability Monitoring

Catalogue

2.1 Real Aperture Radar (RAR)

Real Aperture Radar (RAR) Imaging Schematic

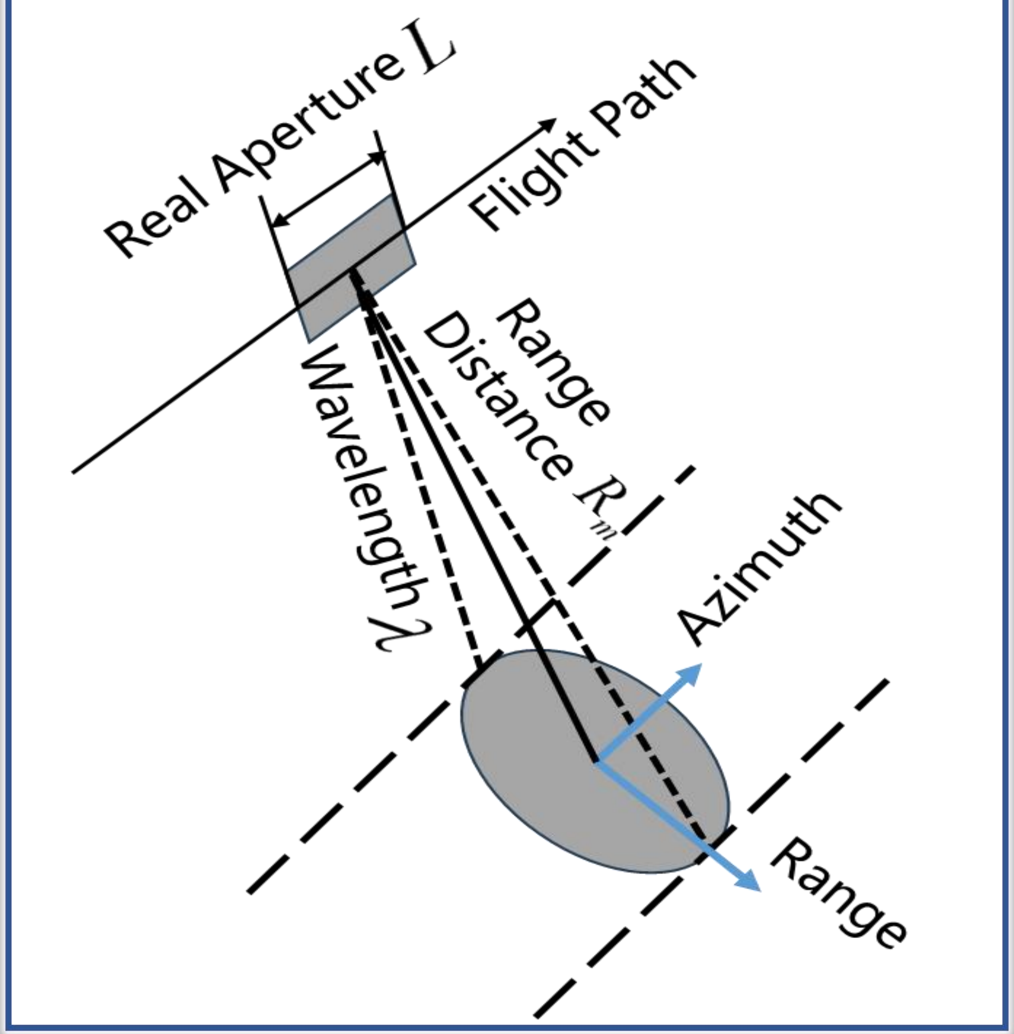

RAR range resolution

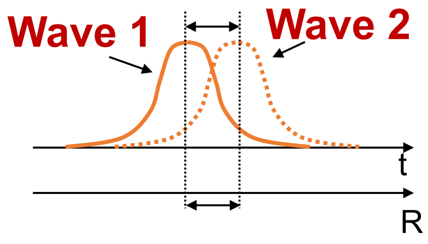

Range resolution ΔR is directly proportional to the radar's pulse width τ .

$$\Delta R = \frac{c \cdot \tau}{2}$$

RAR azimuth resolution

$$\Delta L = R_m \bullet \frac{\lambda}{L}$$

To improve the azimuth resolution in RAR imaging:

- One must decrease the wavelength.
- One increases the aperture length.

2.1 Real Aperture Radar (RAR)

- Decreasing wavelength results in radar signals being reflected by the atmosphere and not reaching the target.

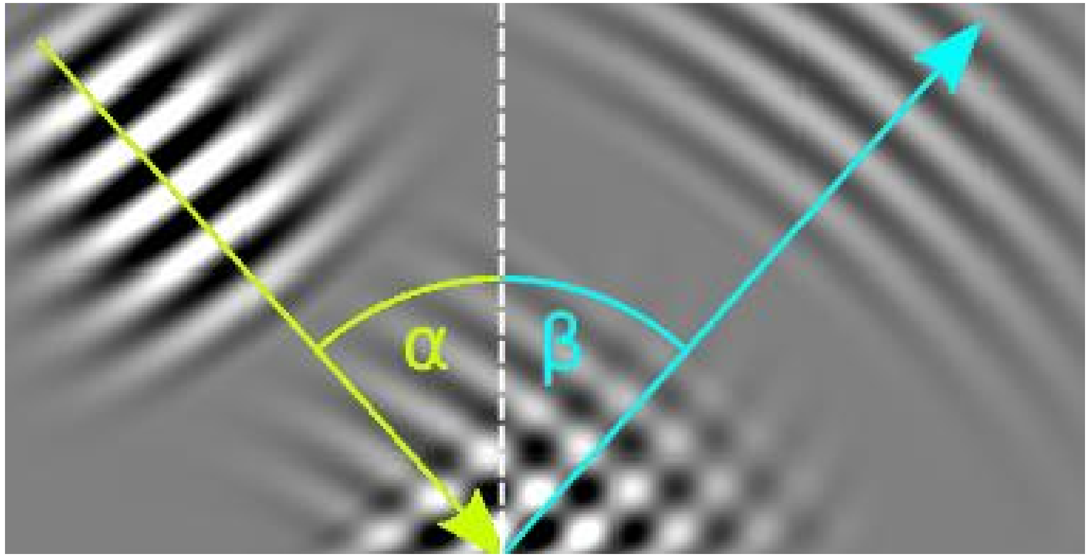

- Increasing the aperture length increases the size of the radar, which is not conducive to mobile measurements.

How to increase the azimuth resolution of a radar while maintaining its original benefits?

2.2 Synthetic Aperture Radar (SAR)

In contrast to real aperture radar, synthetic aperture radar (SAR) simulates a large aperture antenna by emitting radar waves multiple times.

Synthetic Aperture Radar (SAR) Imaging Schematic

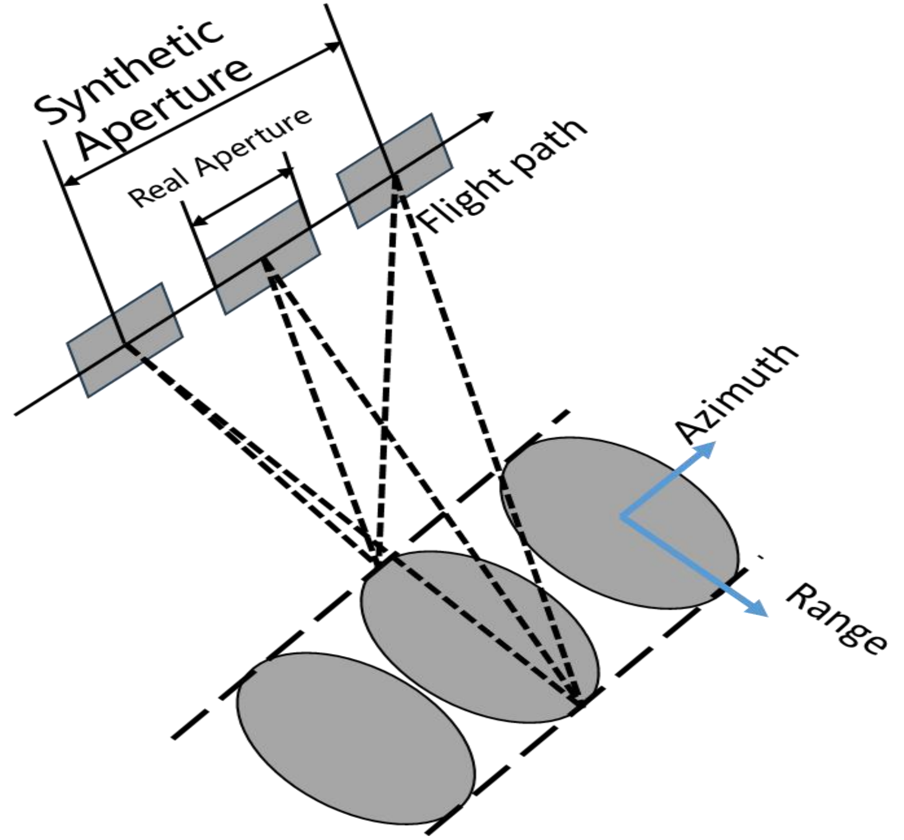

2.2 Synthetic Aperture Radar (SAR)

Optical images are stored in real number format, while SAR images, containing more information, store each pixel in complex number format.

Optical Satellite Image

SAR Satellite Image

2.2 Synthetic Aperture Radar (SAR)

The Euler formula can transform plural into images composed of amplitude and phase values, facilitating subsequent processing.

$$\boxed{a+bi}=\boxed{\sqrt{a^2+b^2}}\bullet e^{i\bullet\boxed{\phi}}$$

Complex Number Image

Amplitude Image

Phase Image

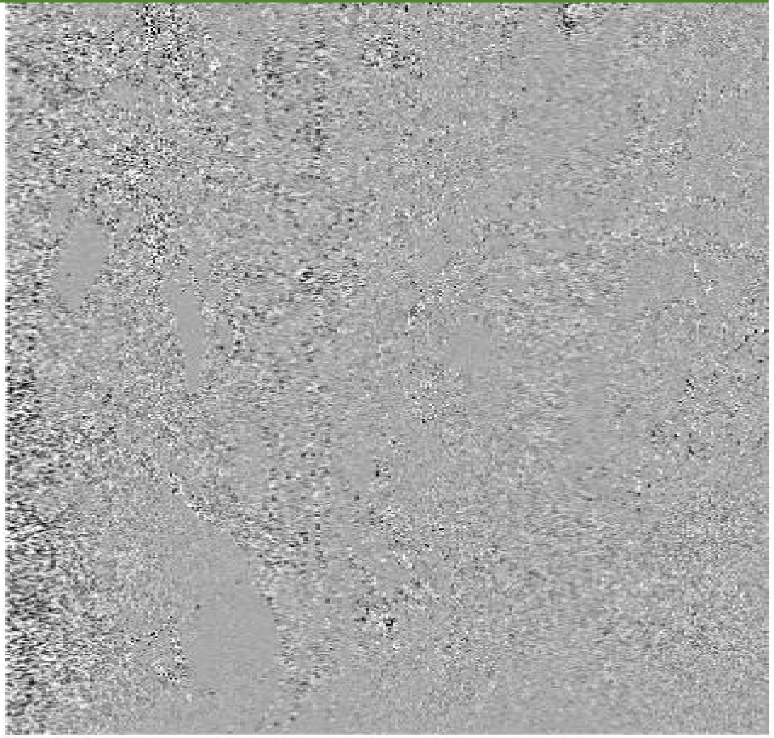

2.3 Interferometric SAR (InSAR)

Interferometric processing is highly suitable for extracting target deformation information from phase data.

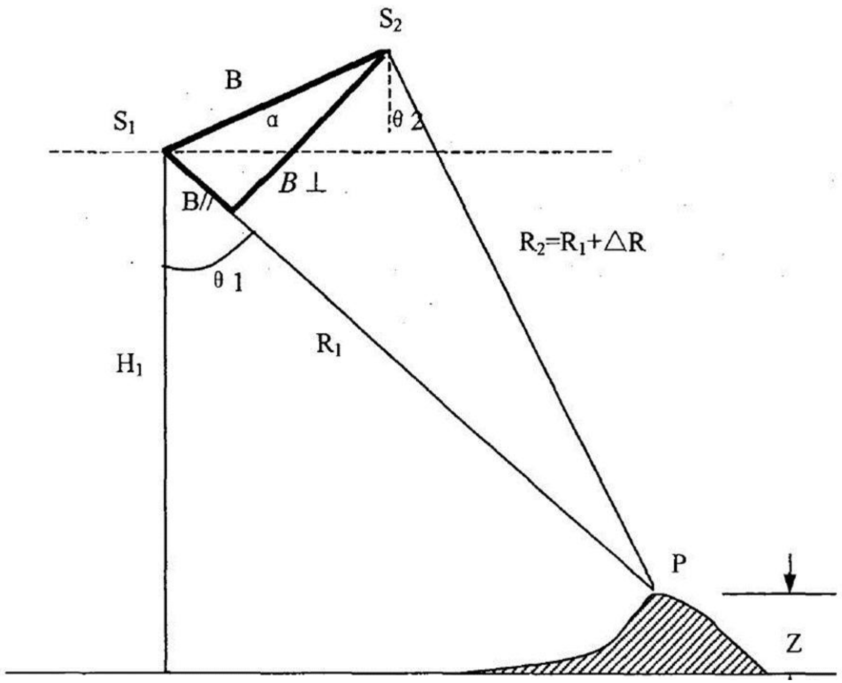

Two phases are superimposed to produce an interferometric phenomenon, which can be seen in the interferogram as colored pixel "stripes" that show the difference in the phase of the signal received by the radar instrument over time, and thus show what changes have occurred in the image.

NASA. https://nisar.jpl.nasa.gov/mission/get-to-know-sar/interferometry/

Extract phase information

$$\begin{cases} \varphi_1 = -\dfrac{4\pi R_1}{\lambda} = -(n_1 \bullet 2\pi + \phi_1) \\ \varphi_2 = -\dfrac{4\pi R_2}{\lambda} = -(n_2 \bullet 2\pi + \phi_2) \end{cases}$$

Phase interferometry

$$\varphi_{Int} = \varphi_1 \times \varphi_2^*$$

Interferogram

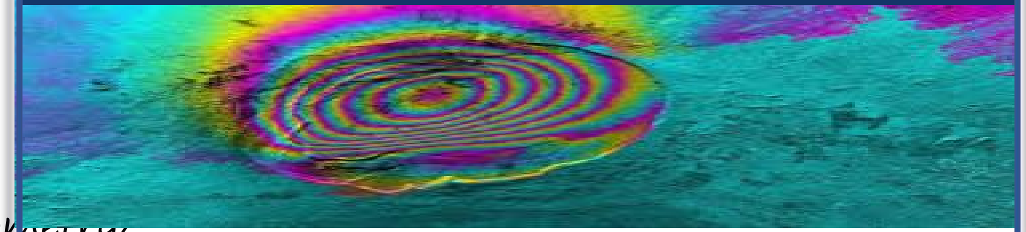

2.3 Interferometric SAR (InSAR)

Continuous interferometric monitoring allows us to track the region's movement or deformation over time.

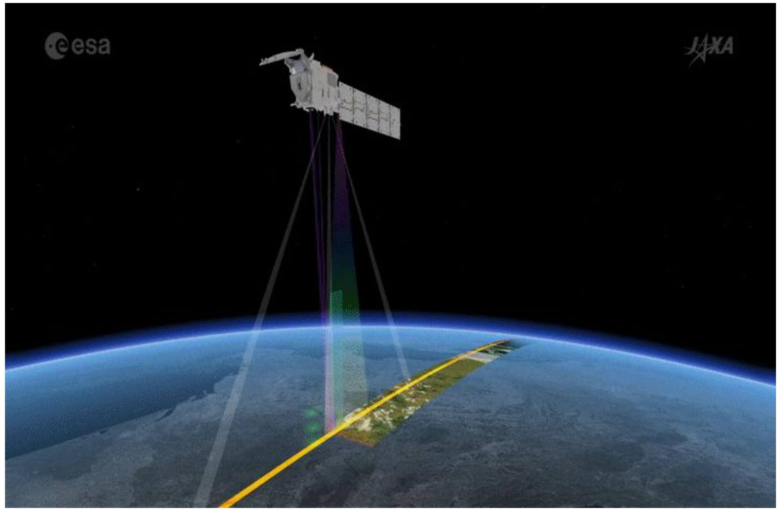

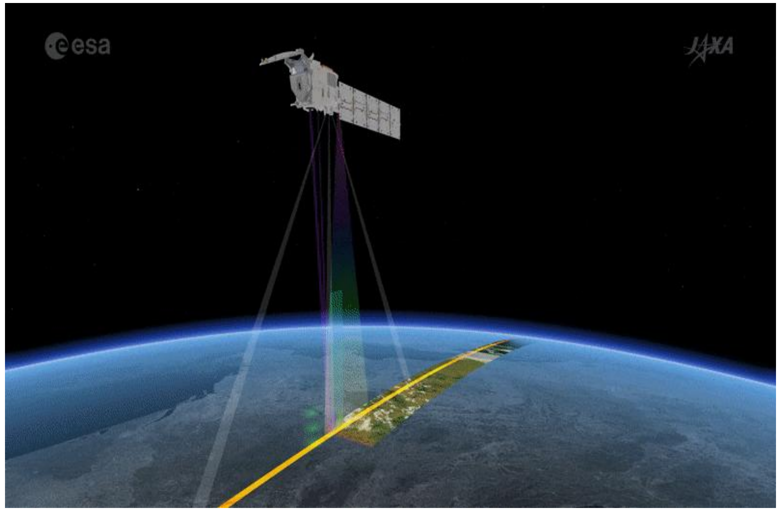

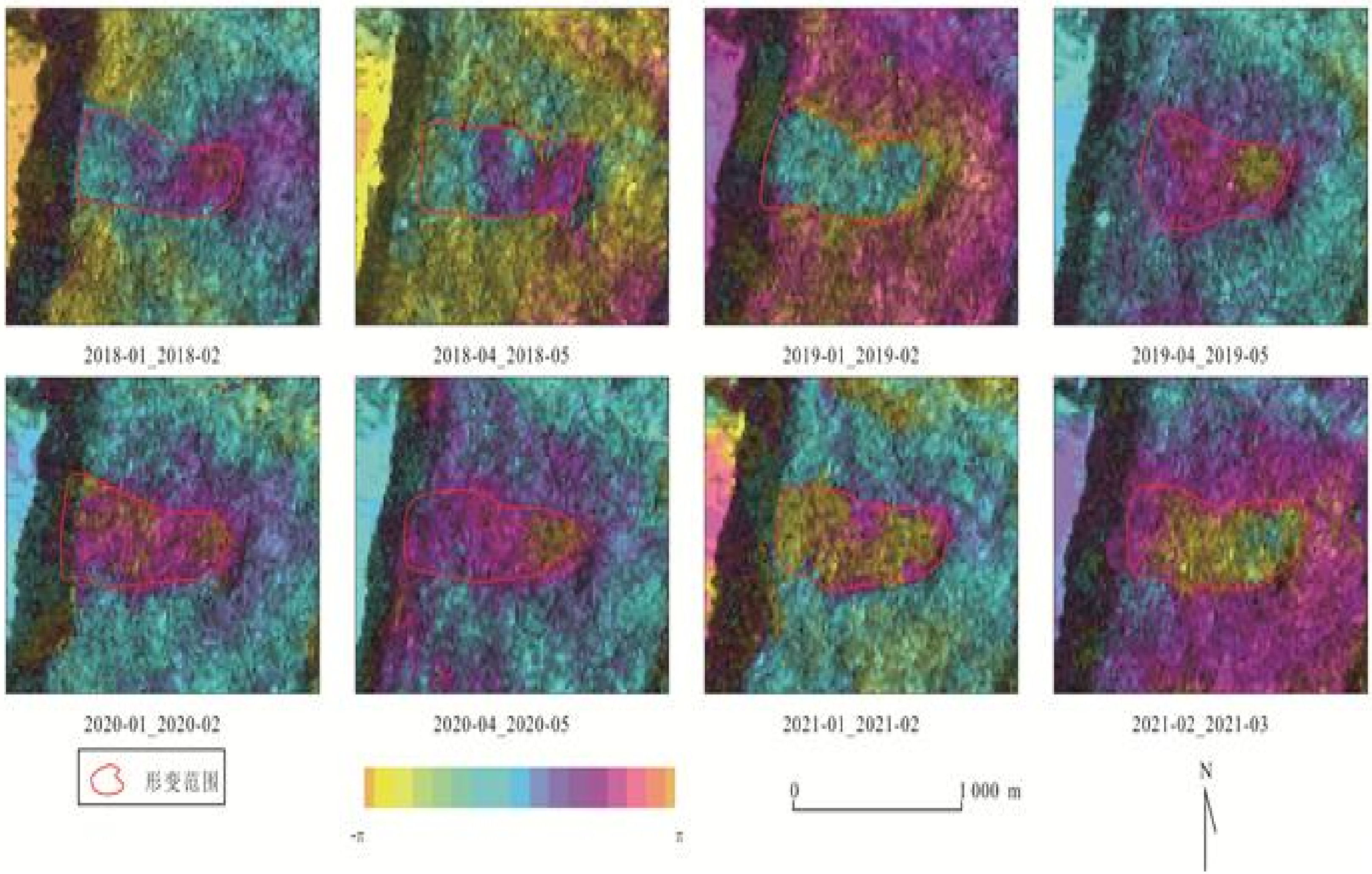

2.3 Interferometric SAR (InSAR)

$$\varphi_{Int} = \boxed{\varphi_{\mathrm{ref}}} + \boxed{\varphi_{\mathrm{top}}} + \boxed{\varphi_{\mathrm{def}}} + \boxed{\varphi_{\mathrm{atm}}} + \boxed{\varphi_{\mathrm{noise}}}$$

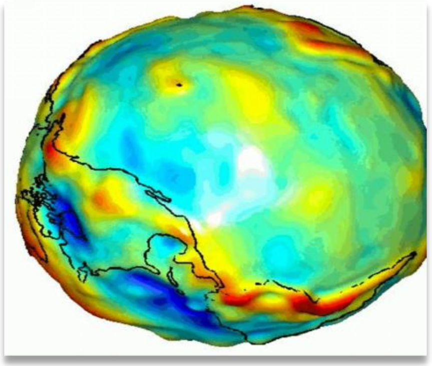

Reference ellipsoid phase

Phase caused by slant range changes on the reference ellipsoid, which can be eliminated by the orbit parameters and geodetic datum calculation.

Terrain phase

Phase caused by terrain elevation changes, which can be corrected by introducing external DEM data.

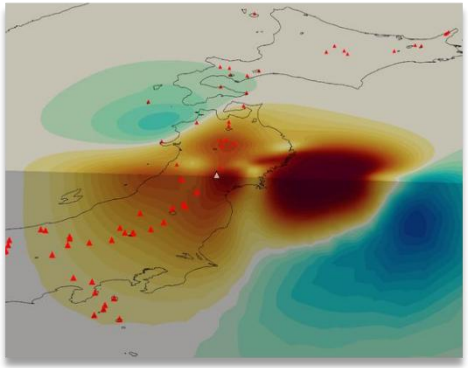

Deformation phase

Phase changes caused by surface deformation are the main targets for InSAR monitoring.

Atmospheric phase

Factors affecting the stability of InSAR results.

Noise phase

Random phase caused by system thermal noise and other factors, which can be reduced by filtering and other methods.

2.4 Permanent Scatterers InSAR (PS-InSAR)

Persistent Scatterer (PS) points are stable reflectors in InSAR image sequences, often artificial structures like buildings or natural objects like rocks. Amplitude dispersion analysis can identify PS points in InSAR images.

Amplitude dispersion analysis $\bar{a} \ge \bar{A} + \sigma_A \;\&\; D_{amp} = \frac{\sigma_{amp}}{\bar{a}} \le 0.25$

2.4 Permanent Scatterers InSAR (PS-InSAR)

After selecting PS points, differential methods are used to establish regression models between adjacent PS points to remove atmospheric phase.

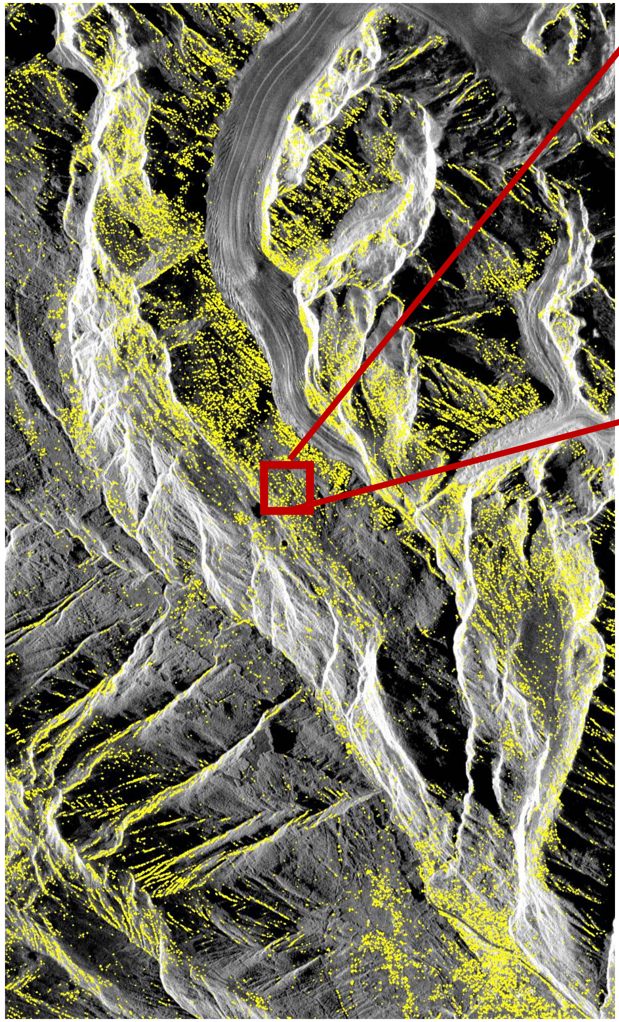

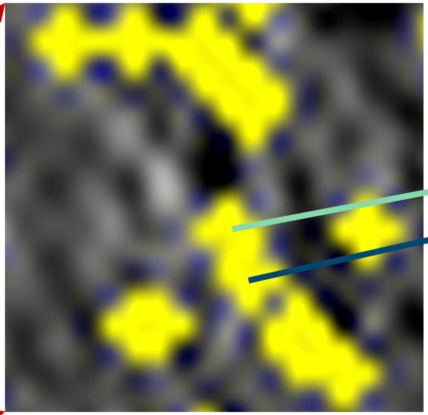

$$\Delta\phi(\boxed{x_1,y_1};\boxed{x_2,y_2};T)=\frac{4\pi}{\lambda R\sin\theta}B_\perp\Delta\varepsilon(x_1,y_1;x_2,y_2)$$

$$+\frac{4\pi}{\lambda}T\Delta v(x_1,y_1;x_2,y_2)+\Delta\varphi^{res}(x_1,y_1;x_2,y_2;T)$$

1. Establish differential models between adjacent PS points by maximizing their coherence.

$$\gamma=\left|\frac{1}{M}\sum_{i=1}^{M}(\cos\Delta\omega_i+i\sin\Delta\omega_i)\right|$$

2. Obtain the relative deformation rate $\Delta v(x_1,y_1;x_2,y_2)$ and elevation error $\Delta\varepsilon(x_1,y_1;x_2,y_2)$

3. Obtain the **linear deformation phase φ_{line}** of each point through integration.

2.4 Permanent Scatterers InSAR (PS-InSAR)

After separating the linear deformation phase and elevation error, the residual phase can be represented as

$$\varphi_{res} = \varphi_{noline} + \varphi_{atm} + \varphi_{noise}$$

Eliminate the noise phase

Noise phase appears as high-frequency phase in space. Low-pass filtering the residual map can eliminate noise phase.

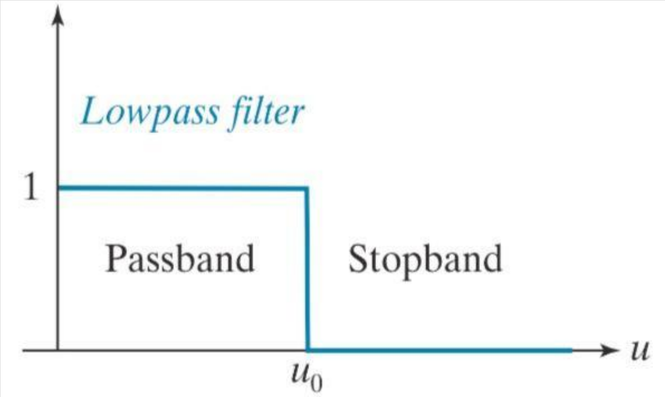

Eliminate the atmospheric phase

Atmospheric phase shows as low-frequency phase over time. High-pass filtering the residual map can remove atmospheric phase.

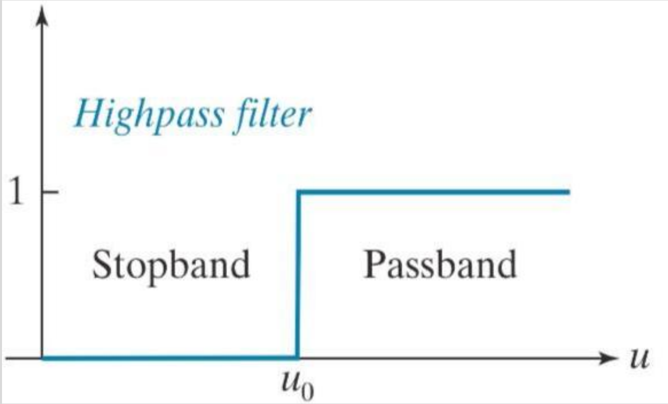

$$\varphi_{def} = \varphi_{noline} + \varphi_{line}$$

2.5 PS-InSAR Shortcomings

The traditional PS-InSAR processing suffers from the insufficient number of PS points and unable to locate damage.

Insufficient number of PS points

Fewer reference PS points for deformation in and around small and medium span bridges

Ignore the buildings structure

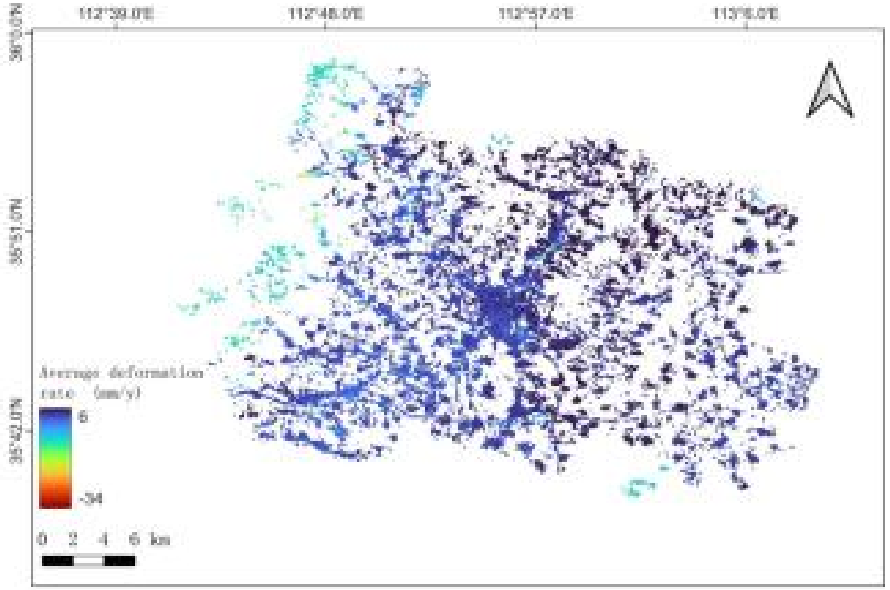

Analyzing PS point subsidence alone can't confirm building damage without considering infrastructure structure.

Yang, F., Zhi, M. & An, Y. Revealing large-scale surface subsidence in Jincheng City's mining clusters using MT-InSAR and VMD-SSA-LSTM time series prediction model. Sci Rep 15, 5726 (2025). https://doi.org/10.1038/s41598-025-88524-0

2.6 PS Points Increase

The interpolation method can effectively improve the coverage of bridges by PS points to obtain the deformation field of bridges.

Quadratic Polynomial Surface Interpolation

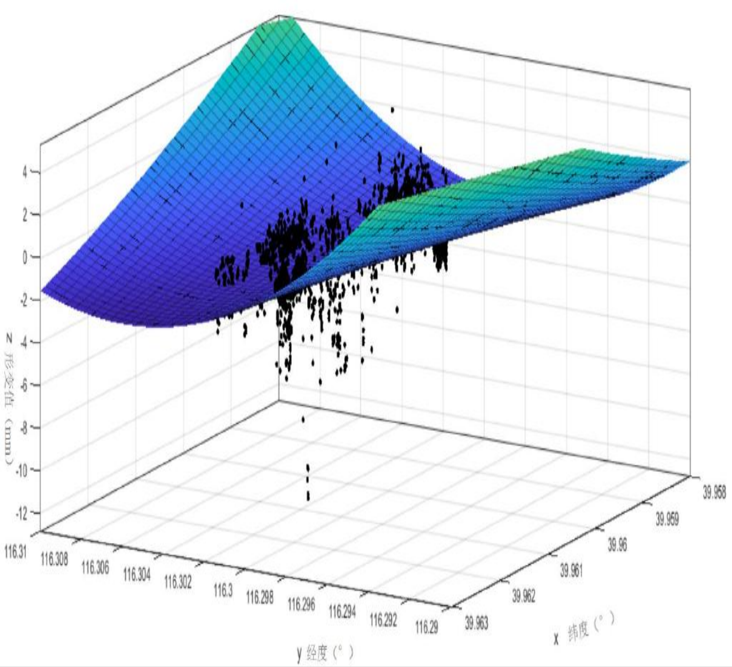

Thin-plate Spline Interpolation

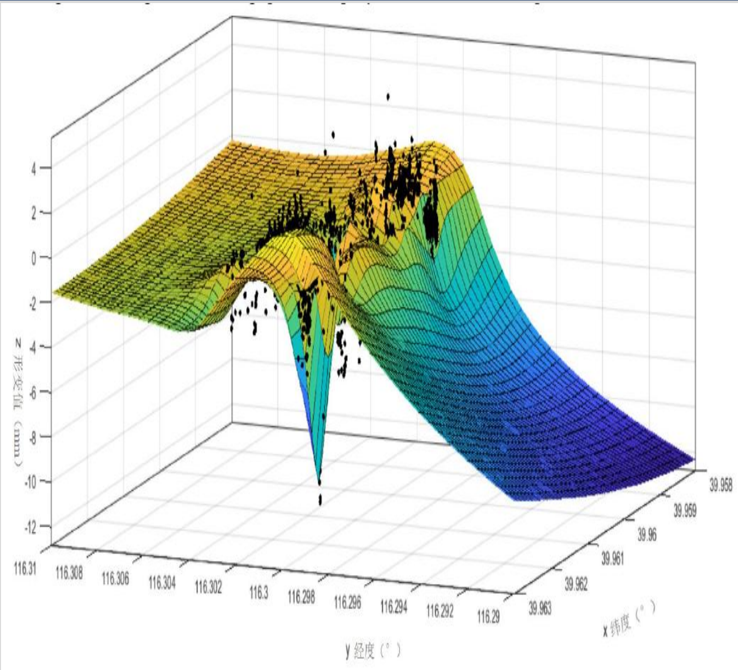

Green’s Function-based Interpolation

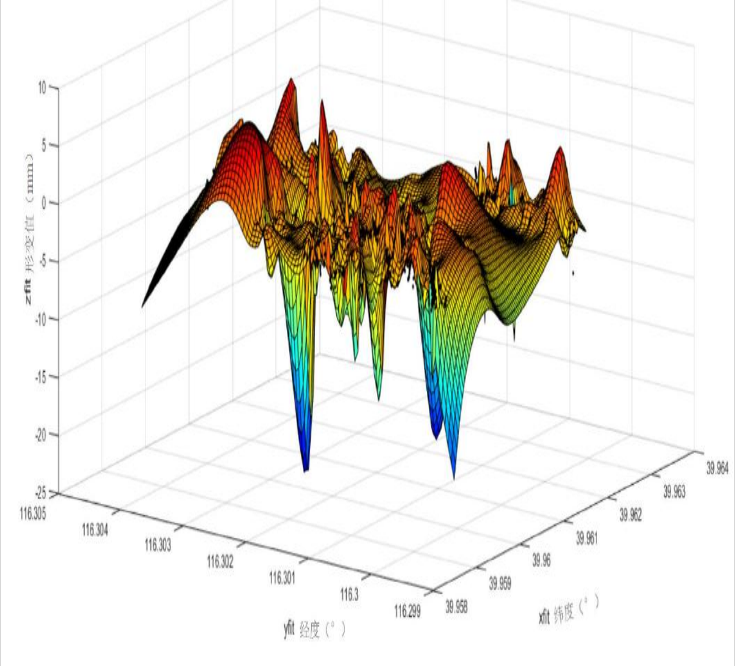

Greene's spline interpolation results in higher accuracy and better fit

2.6 PS Points Increase

According to the deformation field, there is a significant settlement in the middle of the bridge, and the location of the settlement needs to be localized.

Deformation field after interpolating

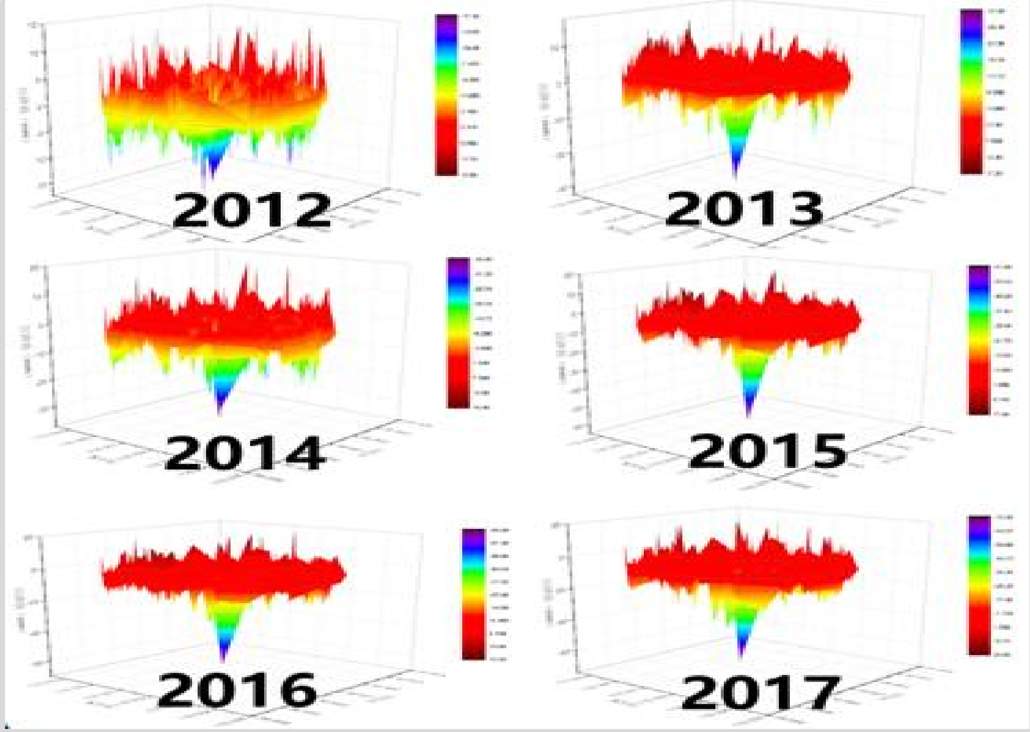

Corresponding deformation position

2.7 Most Unfavorable Condition

Determining the specific location of bridge damage through the most unfavorable condition.

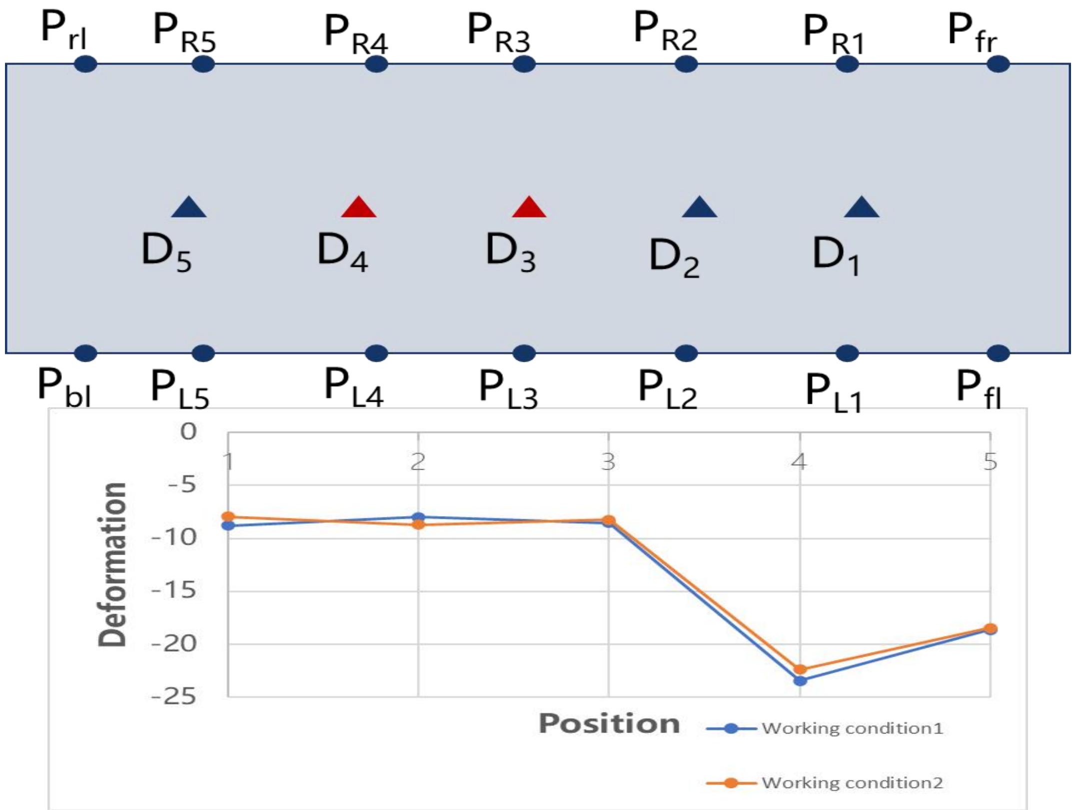

Identification of bridge damage locations for most unfavorable conditions

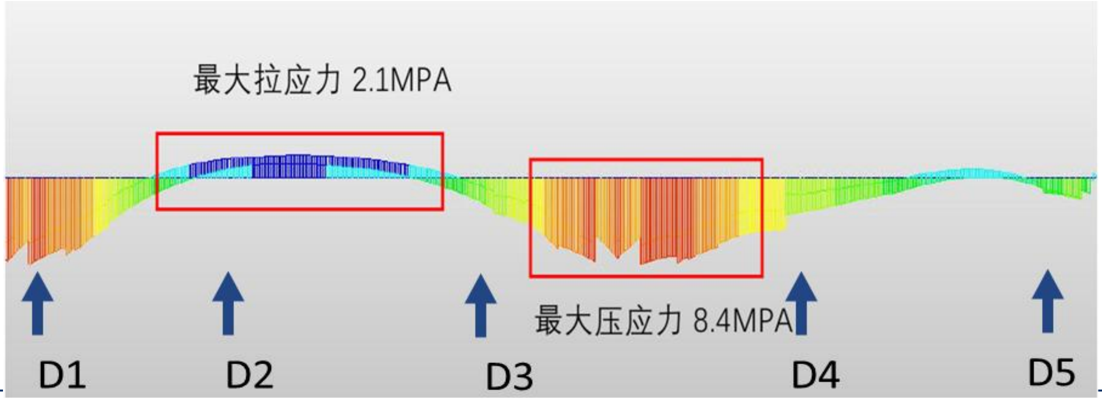

The location of the damage matches the actual situation

Wang, R.J., Zhang, J.M., Liu, X.L.* (2022). A Most-Unfavorable-Condition Method for Bridge-Damage Detection and Analysis Using PSP-InSAR. Remote Sensing, 14(1):137. (SCI)

Catalogue

3.1 Detection of damage deformation in urban infrastructure

In-SAR wide-range measurements

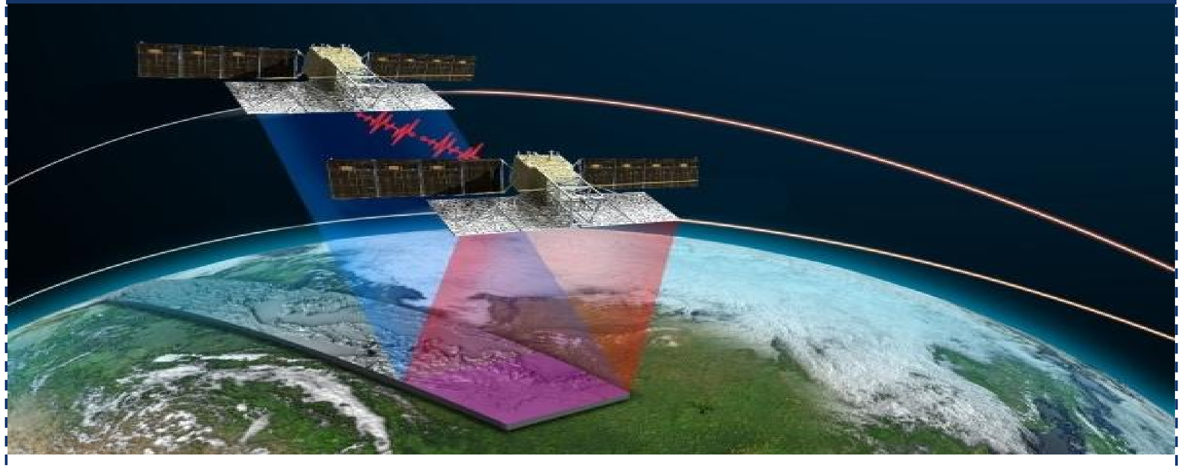

Wide coverage → Mass screening

Efficient data acquisition → Long-term monitoring

Inaccurate monitoring of target-specific deformation

large-scale screening
Identify problematic areas

Challenges in Detecting Damage Areas

intensive measurement → Local damage detection

Deformation monitoring of specific buildings

Medium-scale detailed detection
High-precision data support

Detection of potential damage deformation in specific infrastructures requires smaller scale monitoring.

3.2 Process of TLS for Monitoring Building Damage

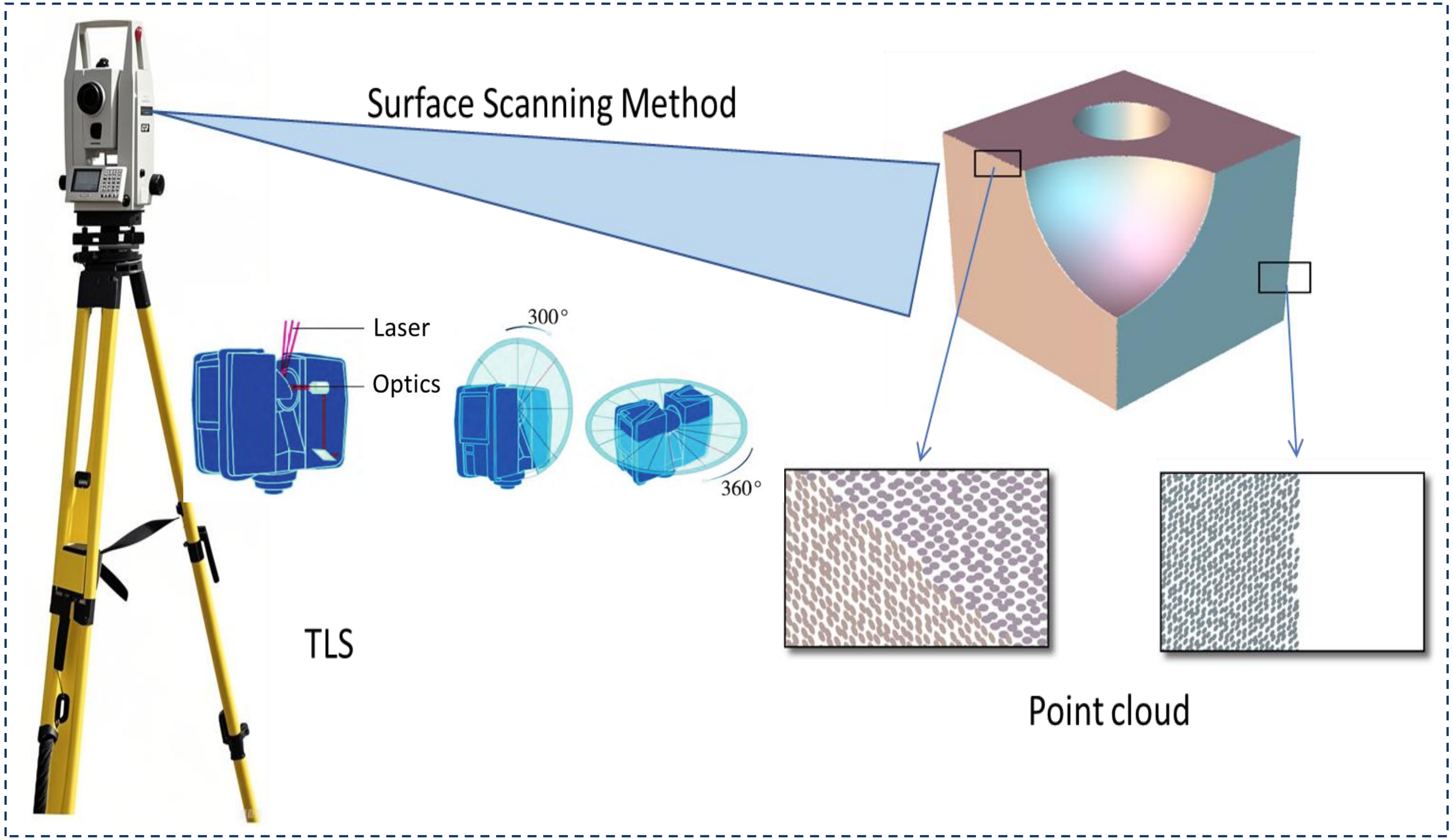

Emit Laser Pulse

Measure Round-Trip Time of Laser Pulse

Determine Angle, Distance, and Coordinates

Generate Point Cloud

Construct 3D Model

By emitting laser pulses, measuring round-trip time, determining angles and distance coordinates, generating point clouds, and constructing 3D models, high-precision monitoring of building damage is achieved.

3.3 TLS Efficiently Enables Infrastructure Potential Damage Monitoring

TLS, known as a real-scene reproduction technology, represents a technological revolution in surveying following GPS.

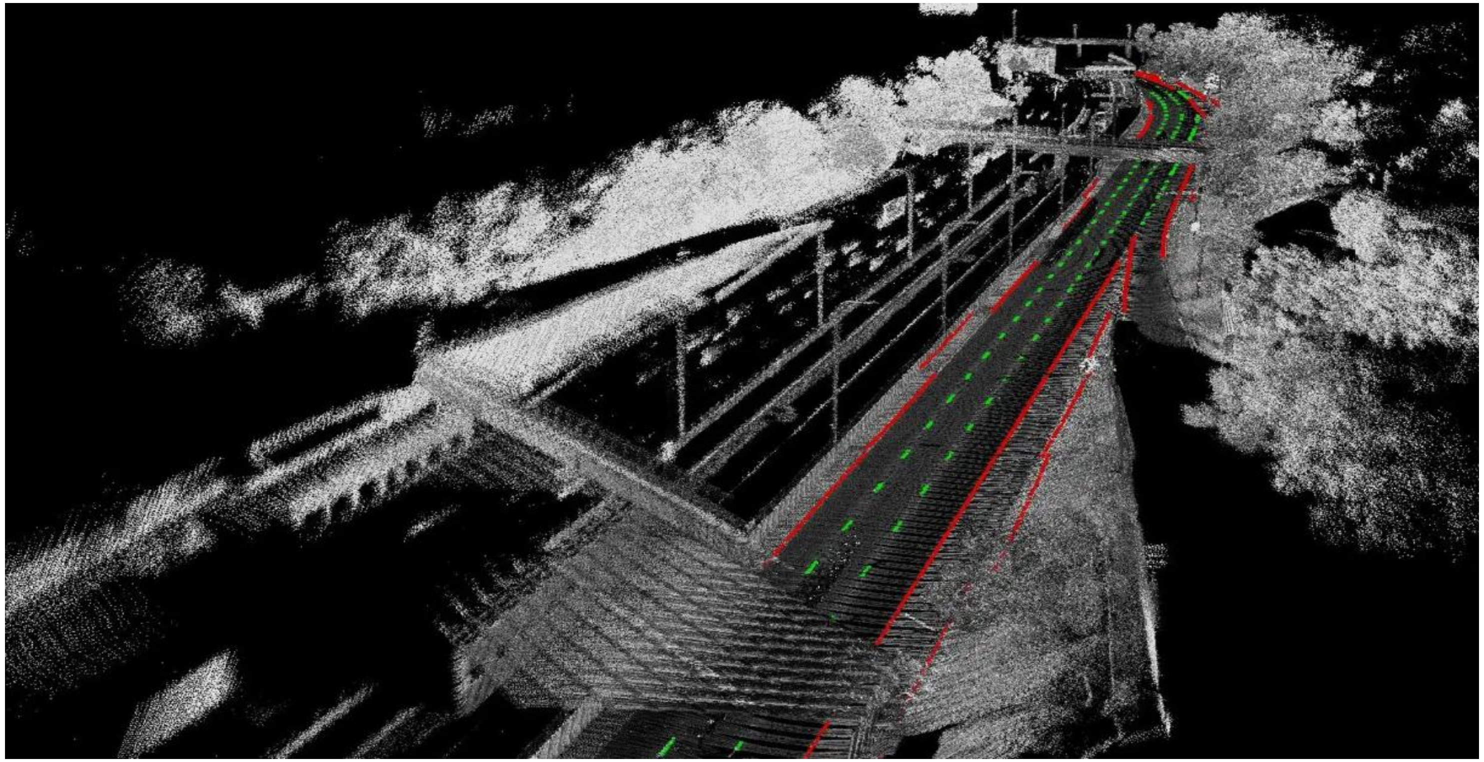

- Face acquisition measurement
- Non-contact
- Intensive Measurement
- High Accuracy

TLS emits laser pulses to generate millimeter-accurate point clouds. Its core, the laser scanner, measures reflection time to calculate distances and create 3D data.

3.4 Breakthroughs and Applications of TLS

Key applications in cultural relic protection

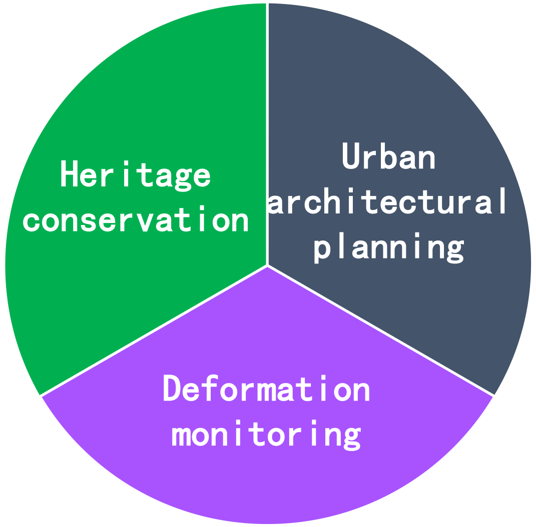

Digital city modeling using 3D laser scanning

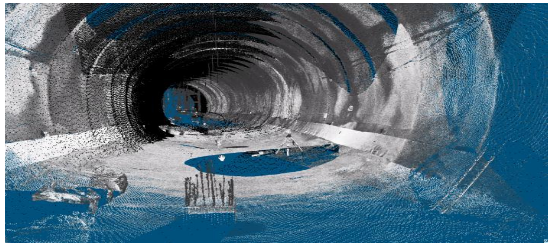

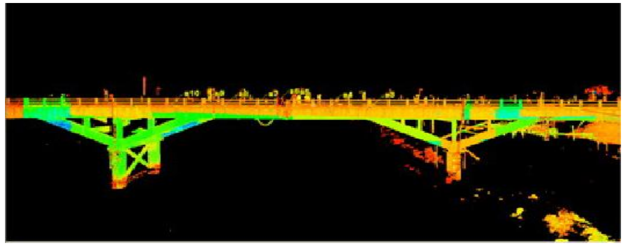

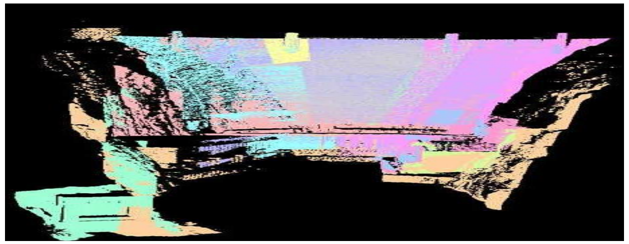

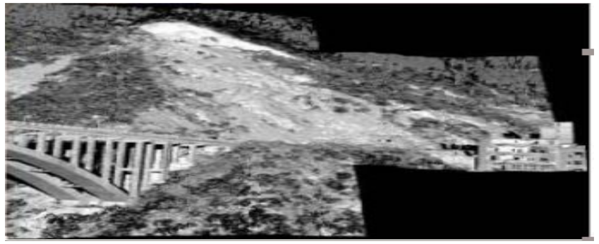

Used for deformation monitoring of tunnels, bridges, dams and landslides, which is of great significance for infrastructure protection.

3.5 Multi-Temporal Point Cloud Acquisition

The methodology involves conducting sequential 3D laser scans of target objects across pre-damage and post-damage states. Each scan cycle requires comprehensive multi-angle coverage from multiple scanning stations, with a minimum 30% overlap between adjacent scan areas to facilitate precise registration. High-end industrial-grade scanners achieve measurement accuracies up to 0.1mm, enabling reliable detection of millimeter-scale structural alterations and damage progression patterns.

Multi-Temporal point cloud

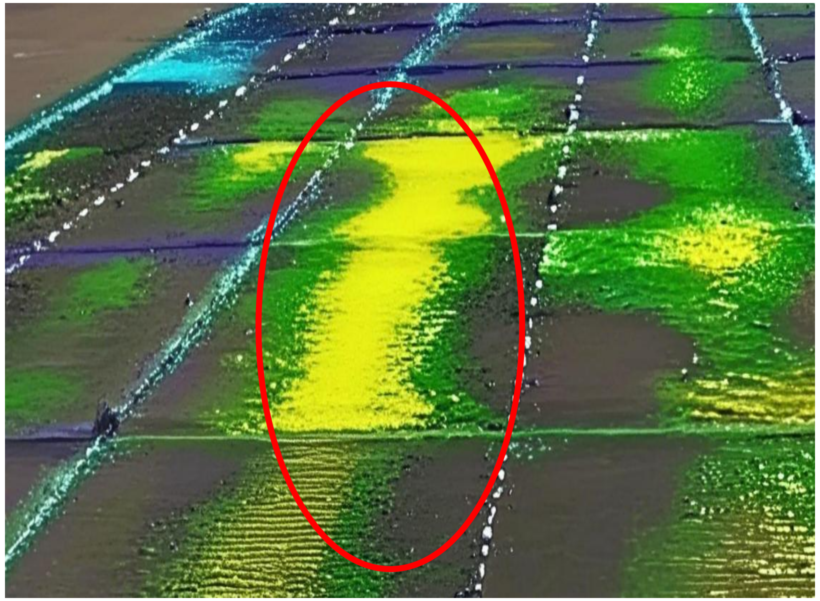

Period of no injury

Damage Area

Comparison of point clouds in different periods

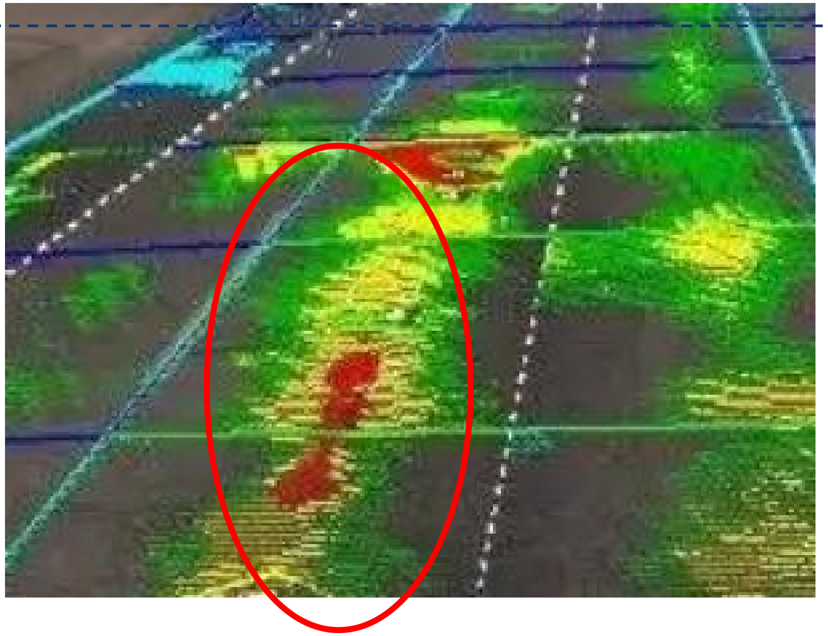

Incidence of damage

3.6 Single temporal Point Cloud Acquisition

Single-temporal point cloud utilizes non-contact 3D laser measurement to efficiently acquire millimeter-level accuracy point cloud models of bridge surfaces. This technique enables the simultaneous capture of structural damage states in a single scanning operation, significantly enhancing both the efficiency and timeliness of detecting potential bridge damage. Through precise point cloud data, it facilitates more detailed and prompt structural health assessments, offering robust data-driven support for bridge maintenance and management.

Single-temporal point cloud

Single-temporal point cloud of the bridge obtained by TLS

↓

Conduct point cloud registration, cropping, and stitching, and calculate point cloud features.

↓

Establish an evaluation criteria related to feature changes for potential damage area detection

Single-temporal →

Real-time

Efficiency

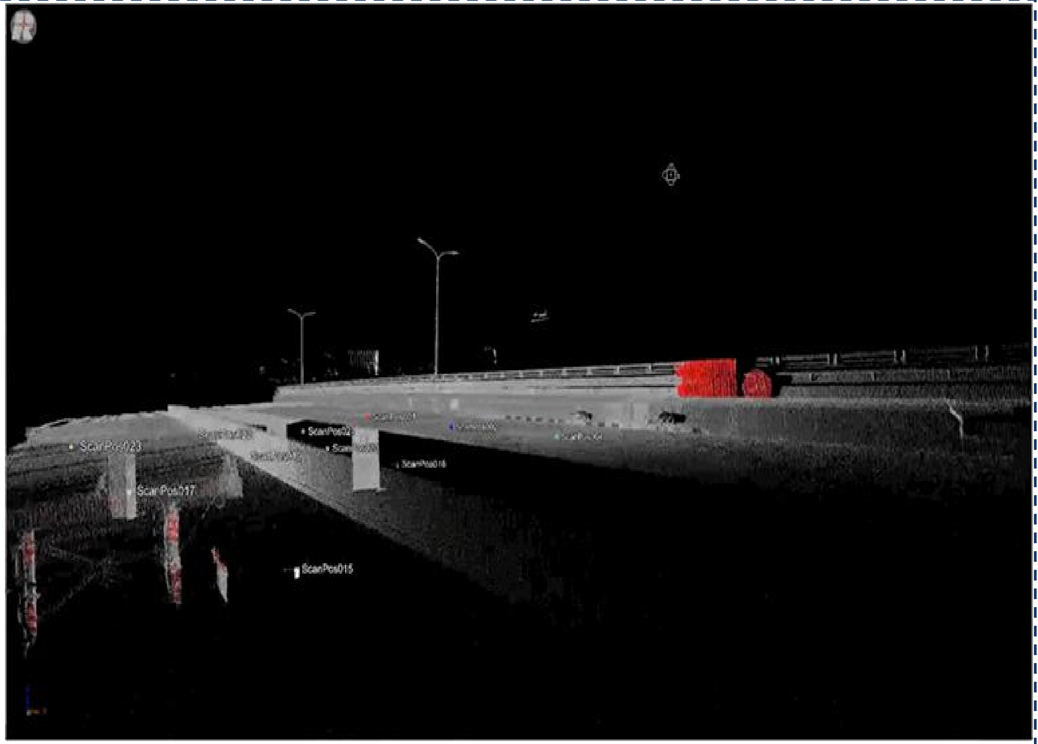

Improve damage detection efficiency

3.7 Single-period point cloud: Efficient Solutions to Traditional TLS Challenges

High-precision 3D modeling of bridge surfaces

Off-target matching

Precision modeling

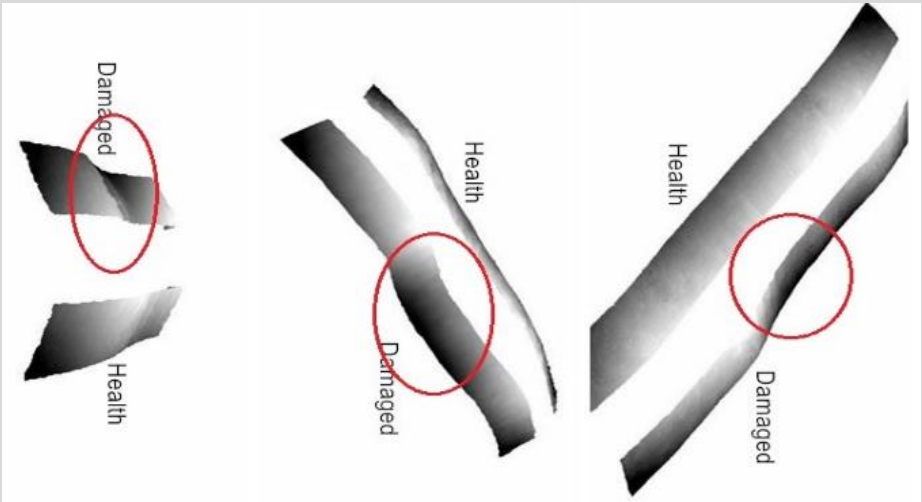

Precision Data

Efficient Detection of Potential Damage Areas

Bridge Features

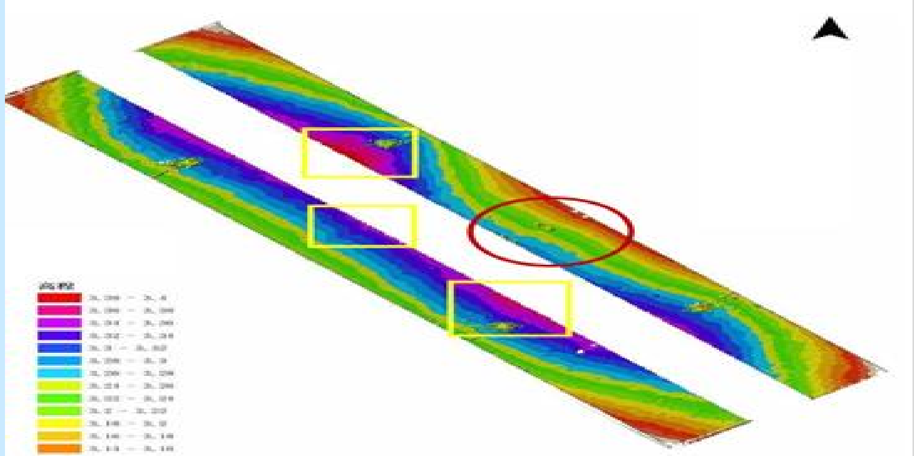

Gaussian curvature

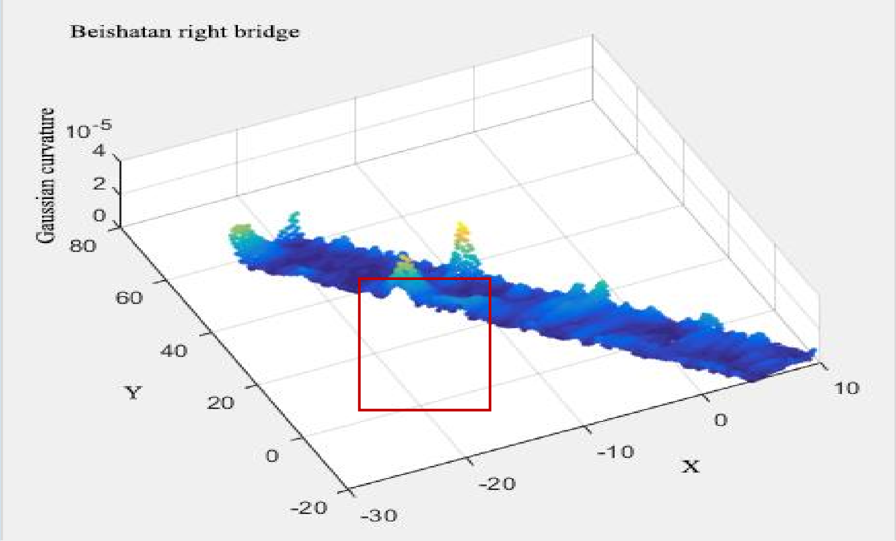

Combining bridge surface modeling and color-based damage detection to achieve efficient damage identification and precise localization in a single measurement.

3.8 Efficient Solutions to Traditional TLS Challenges

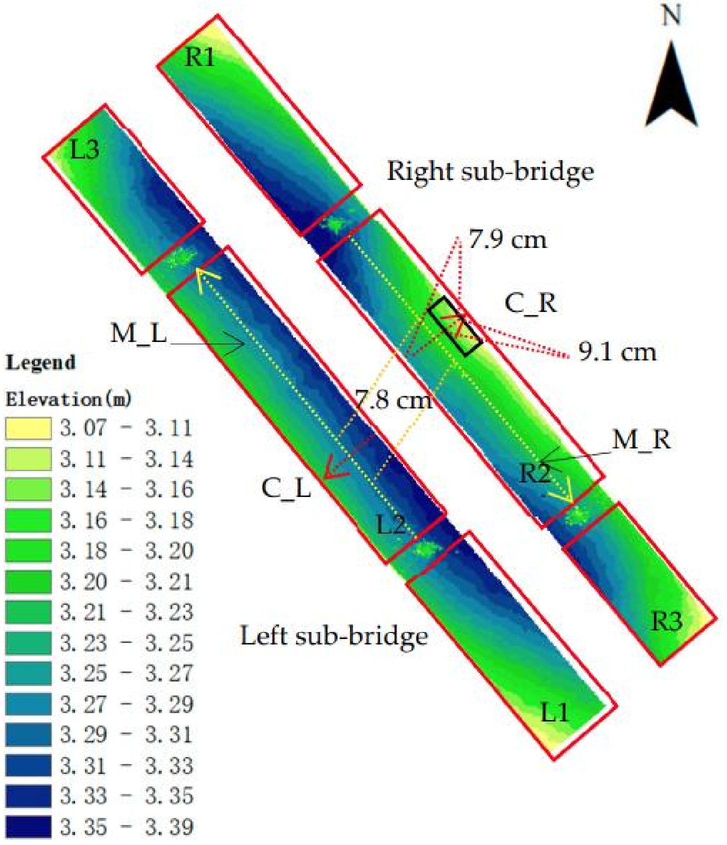

Beishatan Left Bridge

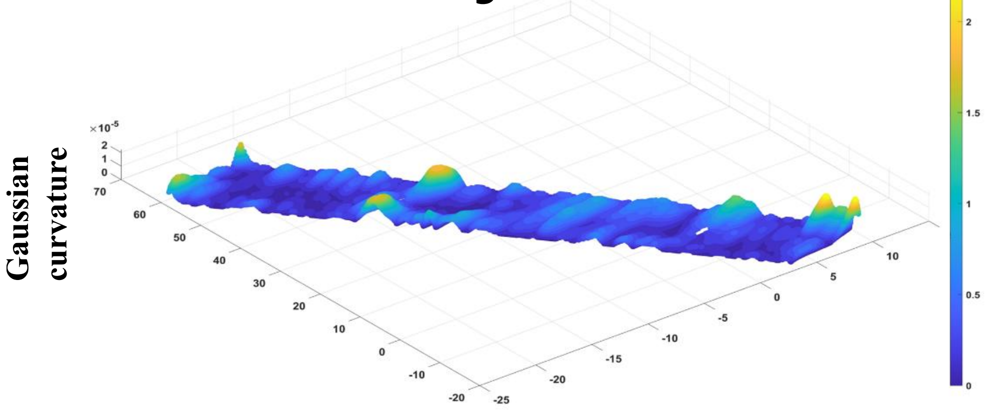

Beishatan Right Bridge

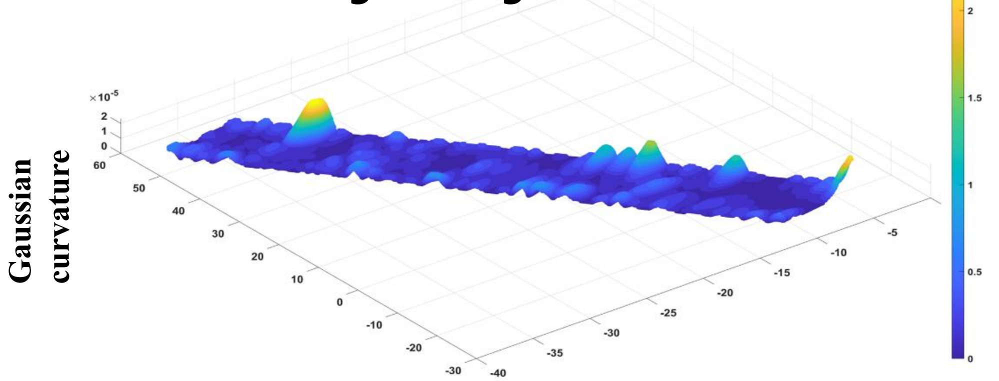

Calculating point cloud curvature can accurately reflect potential damage to the undersurface of bridges

Potential damage area detection of bridges based on single-temporal point cloud, Measurement Science and Technology.

Catalogue

4.1 Introduction to GB-SAR System

TLS performs probing of potential damage areas of the infrastructure to assist GB-SAR in obtaining more accurate damage information to further determine the infrastructure health status.

Terrestrial Laser Scanning

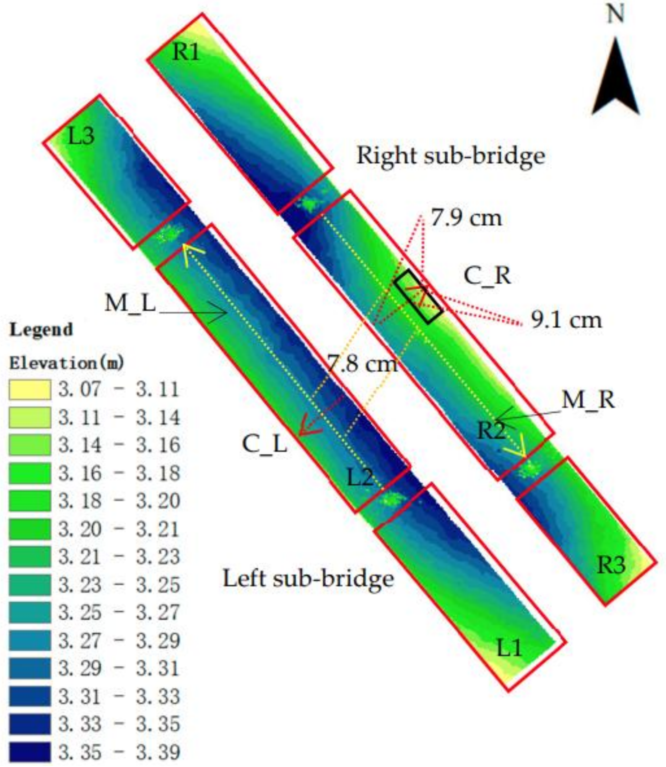

TLS can't accurately determine building damage

Identify potential areas of infrastructure damage

Ground Based Radar

GB-SAR enables more accurate information on building damage

High-precision and high-dynamic microdeformation information acquisition

4.1 Introduction to GB-SAR System

GB-SAR is a ground equipment that utilizes synthetic aperture radar technology, which can be used for high-precision monitoring of small deformation data of urban infrastructure. The sampling frequency can reach 200Hz, and the monitoring accuracy can reach sub millimeter level.

① sensor

② Control compute

③ storage battery

④ Computer power cord

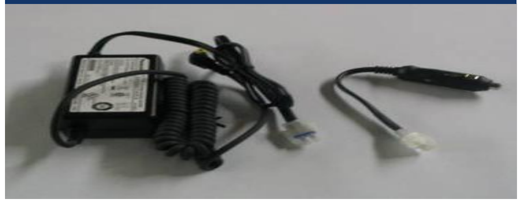

⑤ Instrument and computer connection cables and power supply cables

⑥ tripod

⑦ telescope

⑧ antenna

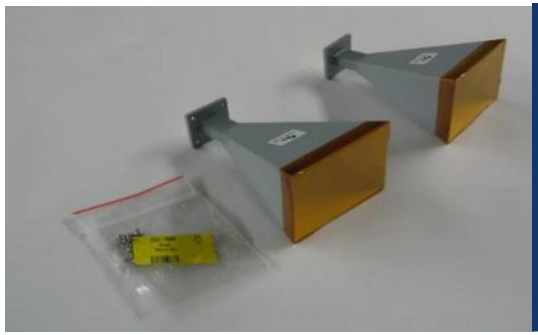

⑨ Tripod rotating head

4.2 Basic principles of GB-SAR

Three core technologies

Technology	Formula	Purpose
SAR	$Ls = \frac{\lambda R}{D}$	Improve the angular resolution of radar
SFCW	$r = \frac{c\tau}{2} = \frac{c}{2B}$	Improve the speed and distance resolution of data acquisition
Interferometry	$d = \frac{\lambda}{4\pi}(\varphi_2 - \varphi_1)$	Measure the small deformation information of the target object

IBIS-S system

- Long distance,contactless
- 24-hour monitoring
- High measurement accuracy of 0.01mm
- Flexible observation methods
- Used under various climatic conditions

4.2 Basic principles of GB-SAR

4.2.1 Synthetic Aperture Radar technology

The meaning of radar is:

RADAR

RAdio Detection And Ranging

Radar is mainly used to detect the presence of target objects and measure the distance between target objects and equipment.

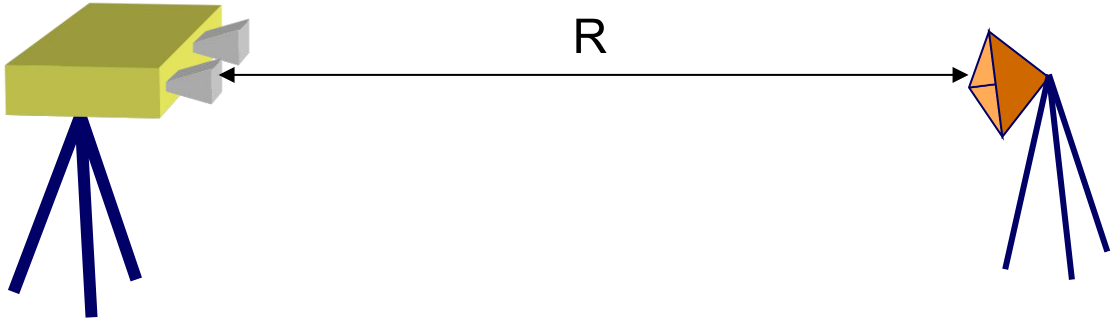

Working principle of pulse radar

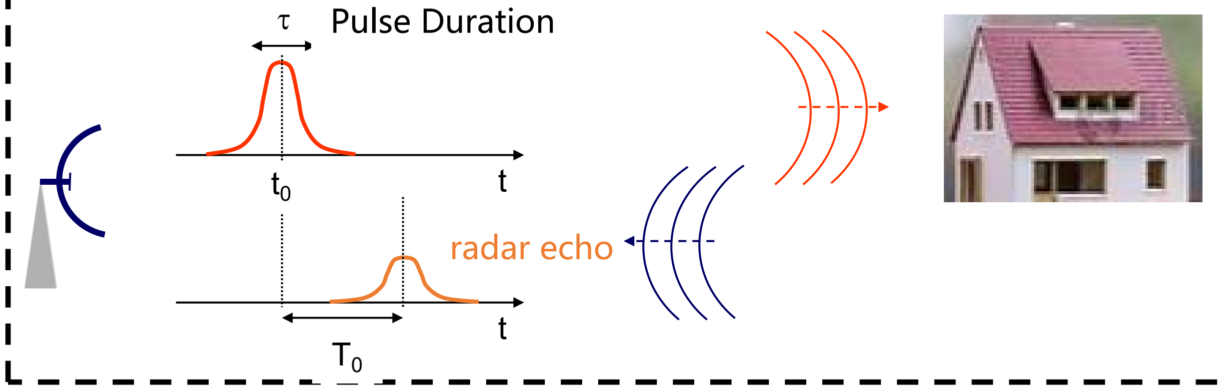

time delay

$$T_0 \rightarrow R_0 = \frac{c \cdot T_0}{2}$$

The concept of range resolution

$$\Delta R = \frac{c \cdot \tau}{2}$$

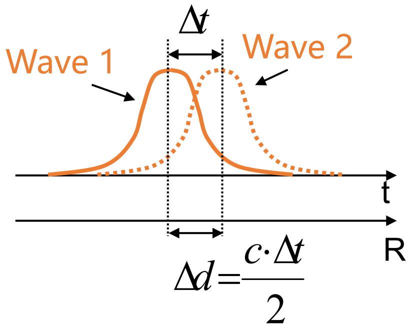

When the following conditions are met, the radar can distinguish between two target objects:

$$\Delta t > \tau \Leftrightarrow \Delta d > \Delta R$$

4.2 Basic principles of GB-SAR

4.2.1 Synthetic Aperture Radar technology

Radar resolution comprises azimuth resolution and range resolution, where smaller numerical values indicate superior resolving performance.

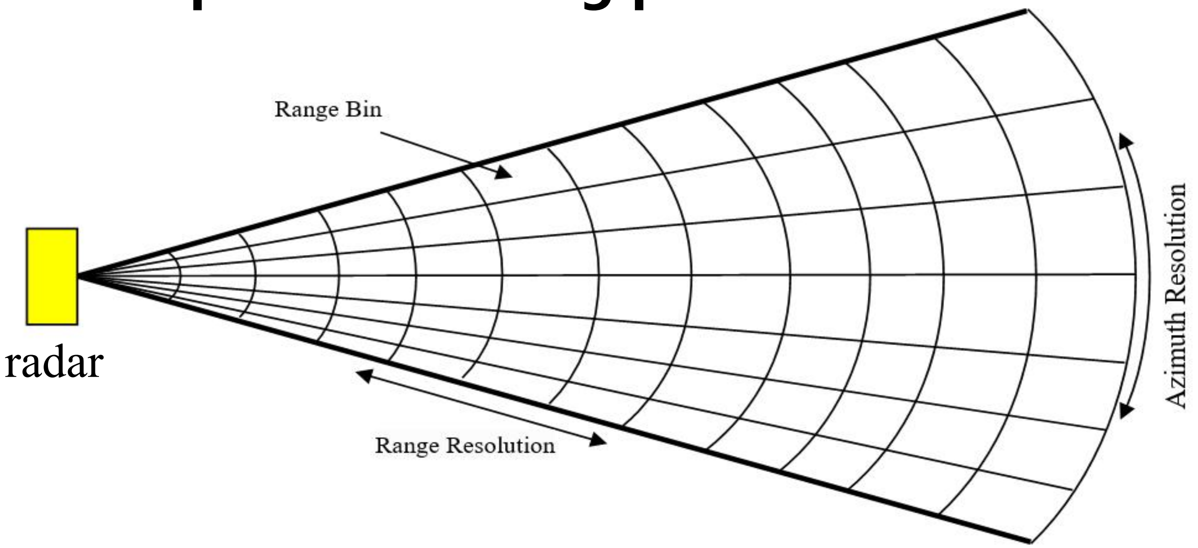

Real Aperture Radar
The resolution of RAR is directly proportional to the length of its antenna. To obtain high-resolution results, RAR requires a significant increase in the antenna's physical dimensions, which imposes substantial constraints on its technological advancement and practical applications.

Doppler Shift

Synthetic Aperture Radar
SAR is a high-resolution radar system that synthesizes a significantly larger equivalent aperture by utilizing a small physical antenna moving along its trajectory. The smaller the physical antenna aperture, the higher the synthetic aperture length, thereby achieving superior resolution.

4.2 Basic principles of GB-SAR

4.2.2 Stepped Frequency Continuous Wave technology

The radar transmission signal of the stepped frequency continuous wave (SFCW) system is a series of continuous waves with discrete increasing frequencies.

Each scan can only proceed to the next scan after the electromagnetic wave reaches the farthest target point R_{max}:

$$T_{tone} > \frac{2R_{max}}{c}$$

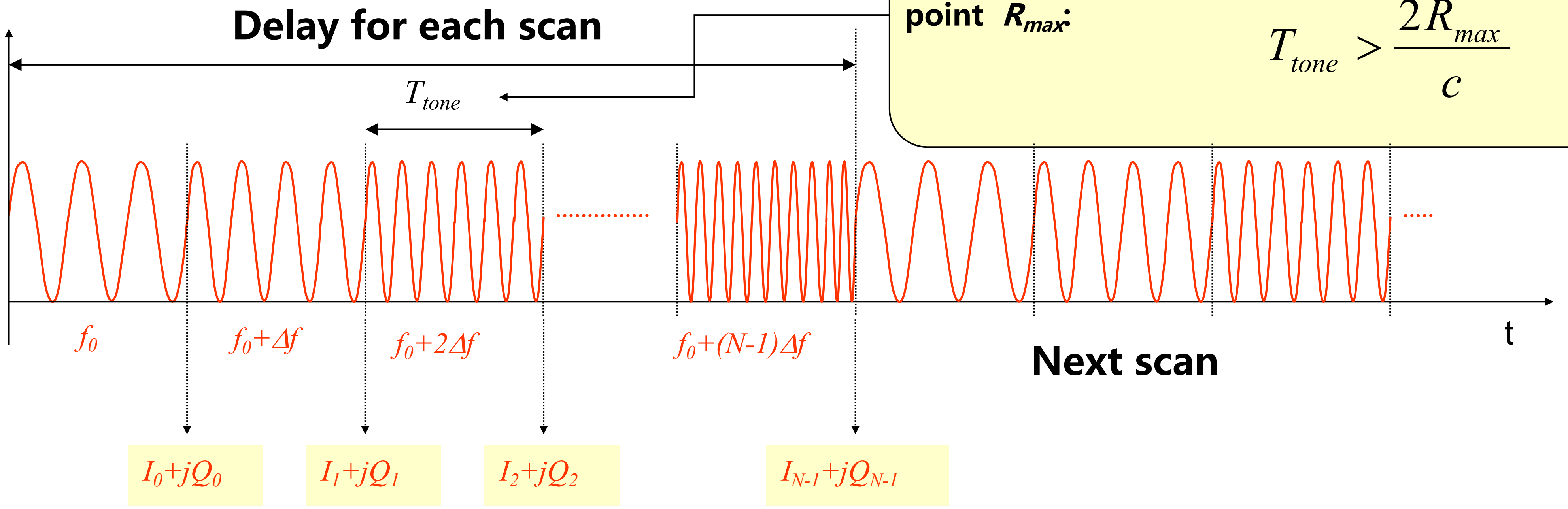

After each sampling, the ground-based radar system can obtain the vector changes of the target object during the sampling time

The system uses inverse Fourier transforms on stepped frequency continuous waves to derive time variations, which are converted into displacement changes of the target.

4.2 Basic principles of GB-SAR

4.2.3 Differential Interference Measurement technique

Differential interferometry compares phase differences of targets at different times to detect minute displacement changes.

Each measurement of the target includes two pieces of information: amplitude An and phase φ_n.

Using SAR and SFCW technologies, IBIS divides the monitoring area into numerous pixel units and obtains displacement data for each.

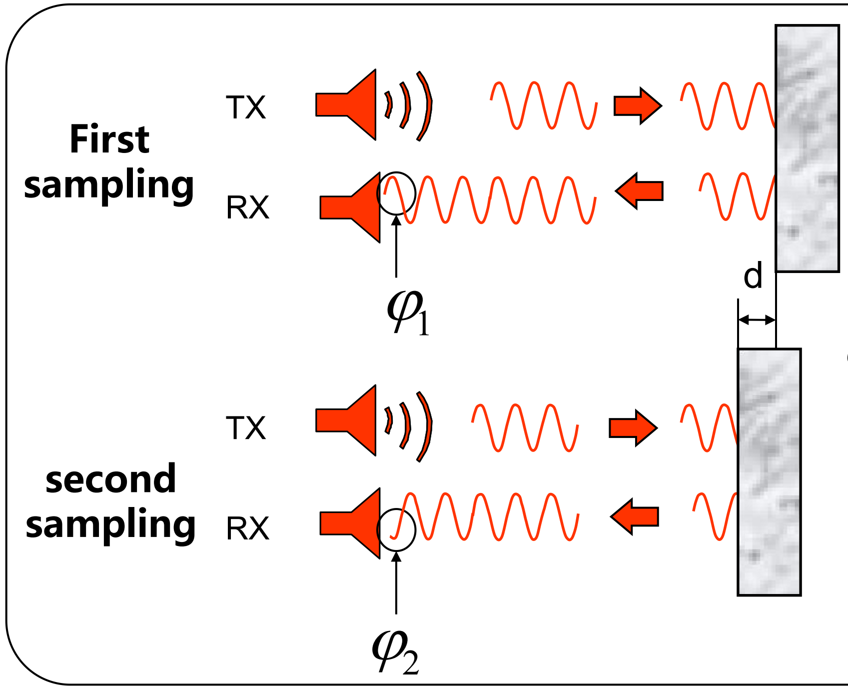

$$d = -\frac{\lambda}{4\pi}(\varphi_2 - \varphi_1)$$

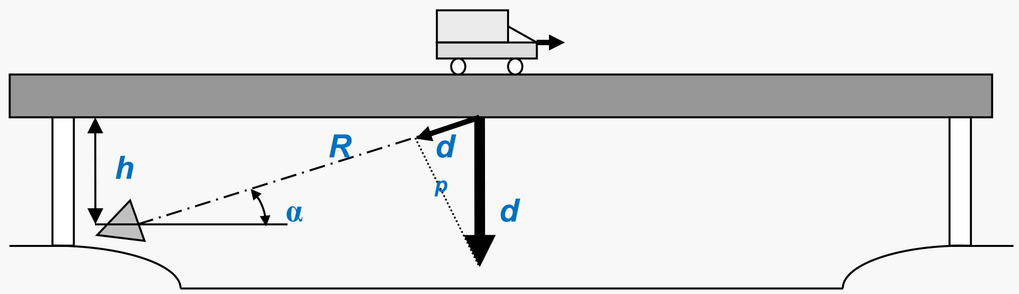

$$d = \frac{d_p}{\sin(\alpha)} \Rightarrow \sin(\alpha) = \frac{h}{R} \Rightarrow d = d_p \cdot \frac{R}{h}$$

- **The displacement change measured directly by IBIS-S is in the range direction (radar line-of-sight).**
- **Processing software can project the target's changes onto other directions.**

4.3 GB-SAR monitoring process

GB-SAR in infrastructure monitoring needs to go through selecting monitoring positions, setting monitoring parameters, recording monitoring results, and doing preliminary pre-processing.

Selecting monitoring positions

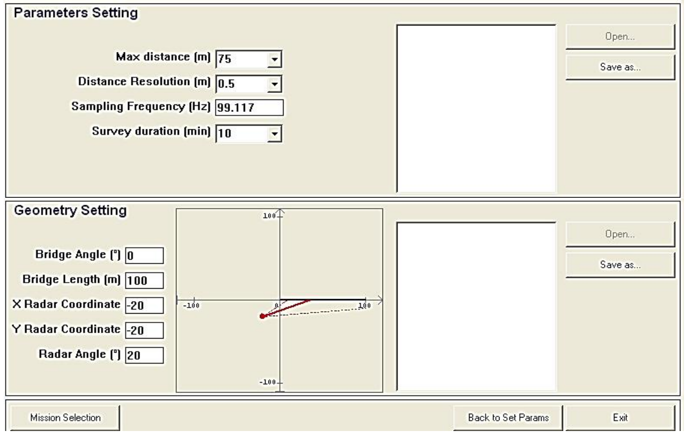

Setting monitoring parameters

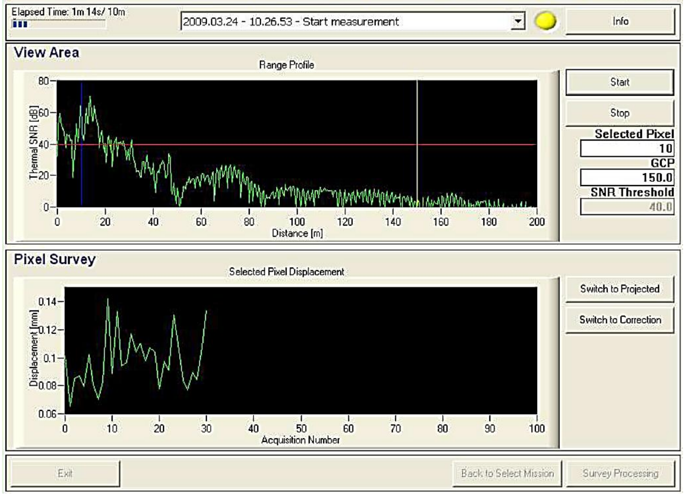

Recording monitoring results

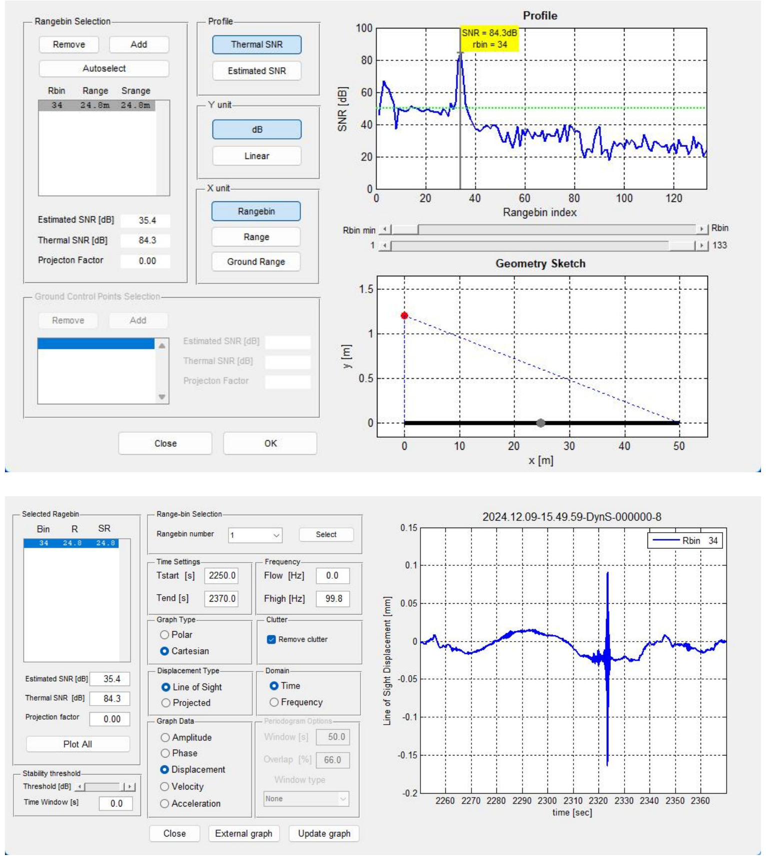

Doing preliminary pre-processing

4.4 GB-SAR atmospheric effect error correction

An optimized Essen-Froome atmospheric model considering bridge geometry and microwave distance was developed to improve infrastructure micro-deformation monitoring accuracy by addressing meteorological effects in ground-based SAR deflection measurements.

Temperature $dt = (\frac{17.23}{T^2}e - \frac{103.49}{T^2} - \frac{991644.96}{T^3}e)$

Atmospheric pressure $dP = (\frac{103.49}{T})$

Water vapor pressure $de = (\frac{495822.48}{T^2} - \frac{17.23}{T})$

$$\begin{cases} \frac{\partial n}{\partial t}\vert(t,P,e) = 1.31 \\ \frac{\partial n}{\partial P}\vert(t,P,e) = 0.35 \\ \frac{\partial n}{\partial e}\vert(t,P,e) = 5.71 \end{cases}$$

season	Temperature	Water vapor pressure	Atmospheric pressure
Spring	1.2268	6.0971	0.3647
Summer	1.6366	5.5513	0.3481
Autumn	1.4646	5.8541	0.3574
Winter	1.2165	6.5979	0.3793

Atmospheric influence mechanism

Theoretical analysis

Water vapor pressure dominates

Experimental verification

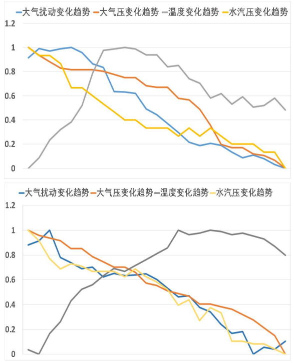

Optimized Correction Model for Atmospheric Parameters

$$d_v = (h - \sqrt{\frac{d_r 2h}{n_i^2 \sin\alpha} + h^2}) - (-0.000002095x^2 + 0.000471x + 0.003807)$$

Mechanism of bridge geometric characteristics influence

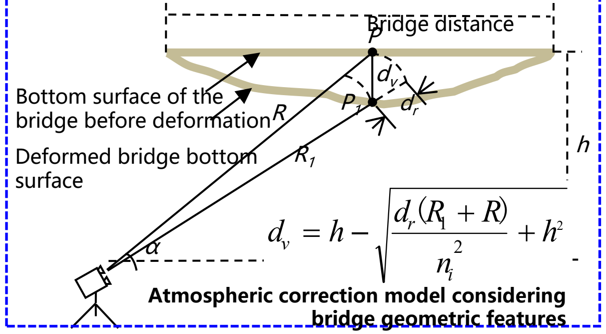

$$d_v = h - \sqrt{\frac{d_r(R_1 + R)}{n_i^2} + h^2}$$

Atmospheric correction model considering bridge geometric features

Feature + Distance

Mechanism of microwave transmission distance influence

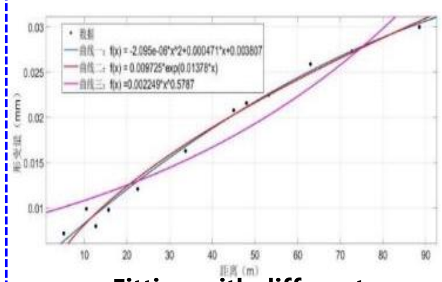

Fitting with different basis functions

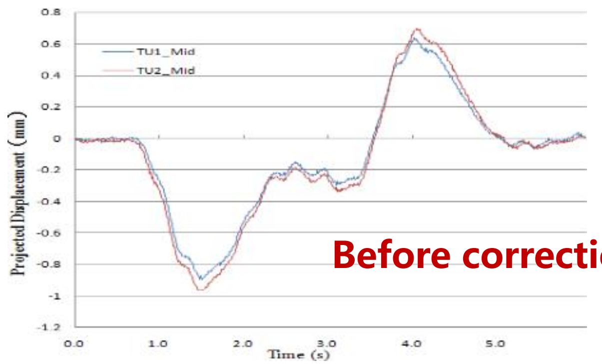

Before correction

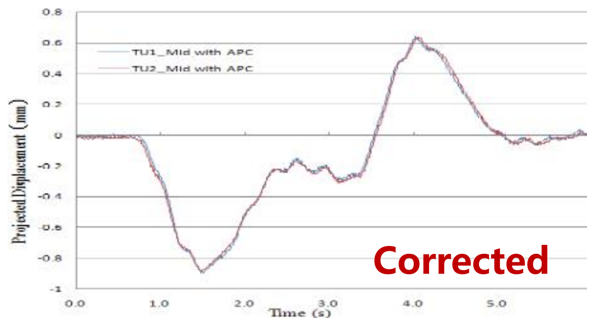

Corrected

This project: increased by 12%

E-F correction: increased by 8.7%

4.5 GB-SAR bridge dynamic deflection signal multi-scale denoisin

A multi-scale hierarchical denoising method was developed to reduce the impact of instantaneous, high-frequency, and low-frequency noise in GB-SAR measurements, achieving a 95% noise reduction and providing accurate data support for damage detection.

T-SOBI instantaneous noise reduction

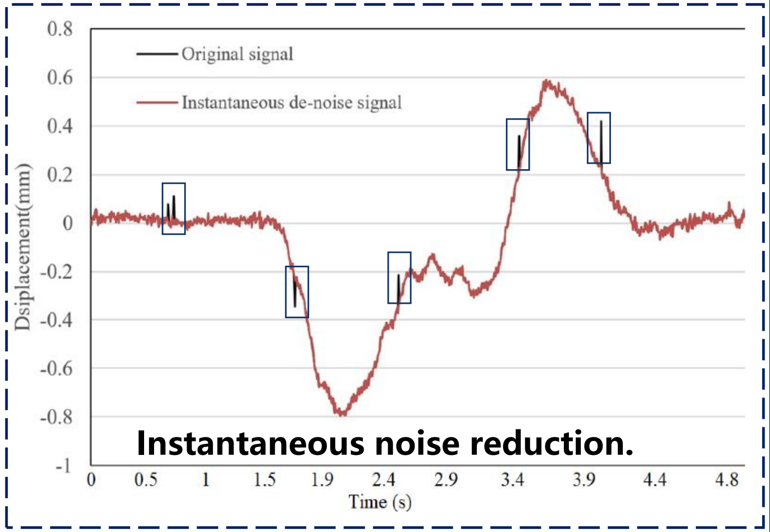

Whitening matrix $W=[(\lambda_1-\sigma^2)^{-\frac{1}{2}}h_1,\dots,(\lambda_3-\sigma^2)^{-\frac{1}{2}}h_3]^T$

Whitening treatment $Z(t)=W*X(t)=W*A*S(t)=V*S(t)$

Variance matrix $R(\tau)=E\left[Z(t)Z^T(t+\tau)\right]=AR_Z(\tau)A^T$

Inverse reconstruction $Y_N(t)=A*Y_Z(t)$

W-ESMD high-frequency noise reduction

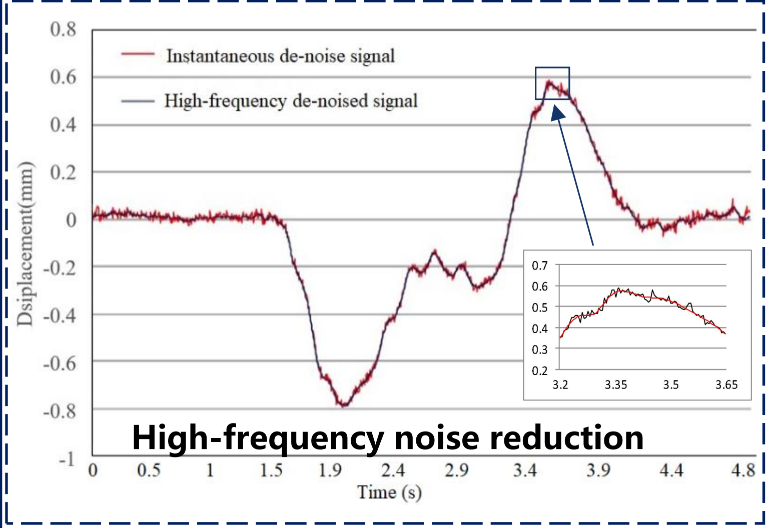

$$\eta_S=\begin{cases}Sign(C)(C-T) & |C|\geq T\\ 0 & |C|<T\end{cases}$$

MF-ESMD low-frequency noise reduction

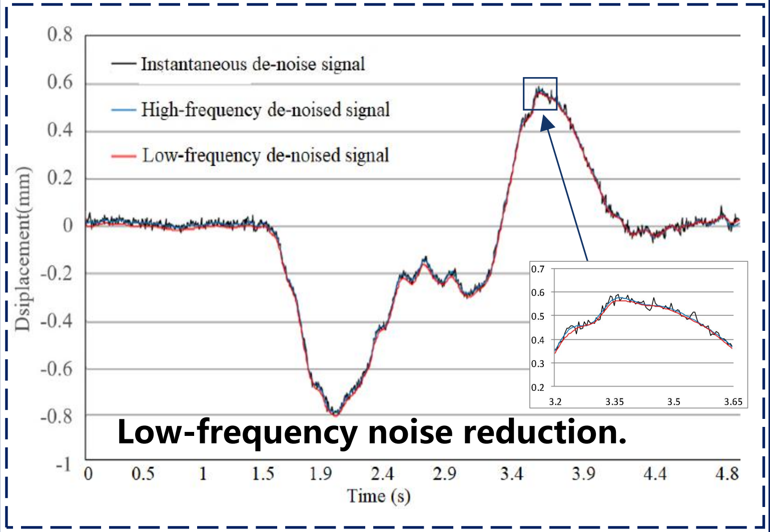

$$s(i)=\rho\left(y(t),IMF_i(t)\right)=1-\frac{6\sum_{i=0}^{N}\left(y(t)-IMF_i(t)\right)^2}{(N^2-1)N}$$

$$s(t)=\frac{1}{2}\left[(y(t)^*\circ g_1\bullet g_2)(n)+(y(t)^*\bullet g_1\circ g_2)(n)\right]$$

4.6 GB-SAR bridge damage identification

A direct interpolation method for instantaneous frequency and total energy multimodal damage identification is proposed to accurately detect damage in non-stationary, nonlinear micro-deformation signals.

Instantaneous frequency calculation of denoised monitoring signals after ESMD decomposition

The left sub-bridge chose Rbin24, with a maximum deflection of 8.63 mm.

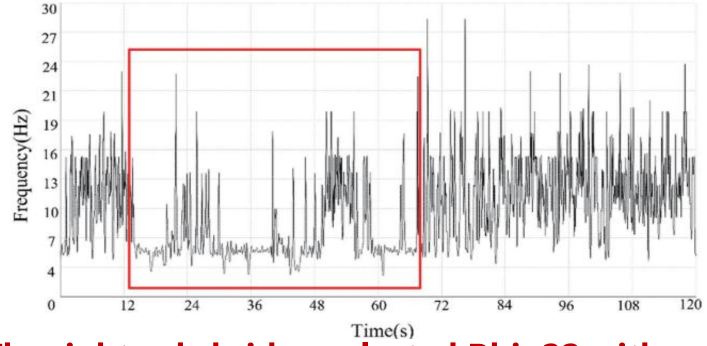

The right sub-bridge selected Rbin22 with a maximum deflection of 13.17 mm.

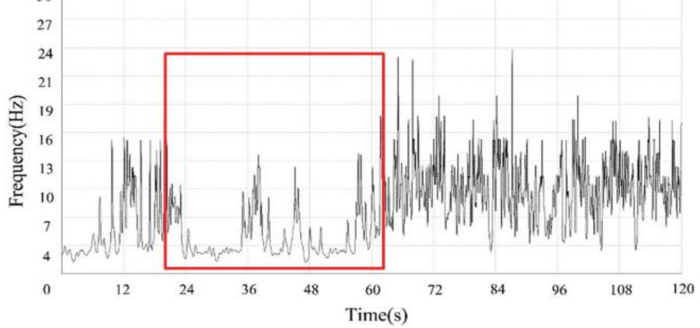

Rbin24 (left) drops from 14–67s, Rbin22 (right) from 18–62s.

Instantaneous total energy integral.

Table 1
Energy integration results of all reflection points of the left sub-bridge.

Reflection points	Rbin8	Rbin9	Rbin10	Rbin11	Rbin12	Rbin13	Rbin14	Rbin15	Rbin16	Rbin17	Rbin18
Horizontal distance (m)	1.6	3.3	4.6	5.6	6.6	7.5	8.4	9.3	10.1	10.9	11.8
Energy integration	2.7689	10.3612	8.1392	10.5119	14.1569	17.3247	15.6212	28.2039	22.3829	23.3708	19.9832
Reflection points	Rbin19	Rbin20	Rbin21	Rbin22	Rbin23	Rbin24	Rbin25	Rbin26	Rbin27	Rbin28	Rbin29
Horizontal distance (m)	12.6	13.4	14.2	15.0	15.8	16.6	17.3	18.1	18.9	19.7	20.5
Energy integration	28.3573	26.8473	21.0767	25.5452	45.3735	140.9261	46.7376	21.3127	15.621	22.2915	22.7781

Zuozi Bridge: Energy change is gradual, with the maximum energy integral at Rbin24 reflection point.

Table 2
Energy integration results of all reflection points of the right sub-bridge.

Reflection points	Rbin8	Rbin9	Rbin10	Rbin11	Rbin12	Rbin13	Rbin14	Rbin15	Rbin16	Rbin17	Rbin18
Horizontal distance (m)	1.6	3.3	4.6	5.6	6.6	7.5	8.4	9.3	10.1	10.9	11.8
Energy integration	5.3762	5.0415	5.0442	7.8028	16.9166	20.0845	16.2250	28.9991	117.9819	25.1440	21.4363
Reflection points	Rbin19	Rbin20	Rbin21	Rbin22	Rbin23	Rbin24	Rbin25	Rbin26	Rbin27	Rbin28	Rbin29
Horizontal distance (m)	12.6	13.4	14.2	15.0	15.8	16.6	17.3	18.1	18.9	19.7	20.5
Energy integration	22.3068	20.2216	16.8124	120.8181	6.4011	12.0530	11.7267	19.9687	26.0411	11.6862	5.1193

Right sub-bridge: Significant energy fluctuation, with Rbin22 having the highest energy near the reinforcement jack (15.2m).

Multi-phase data builds a bridge for long-term health assessment systems

Single-stage data monitoring
Suitable for emergencies or preliminary assessments, conducted quickly after a bridge incident to evaluate immediate damage.

Multi-period data monitoring:
Track deformation trends over multiple periods for a comprehensive health assessment. By analyzing changes across different timeframes, it enables the establishment of a long-term evaluation system.

Catalogue

5.1 Research Background

To ensure structural reliability, scaled model shaking table tests were conducted prior to bridge construction. Conventional contact-based measurement methods present installation challenges and may potentially interfere with structural performance.

(a)

(b)

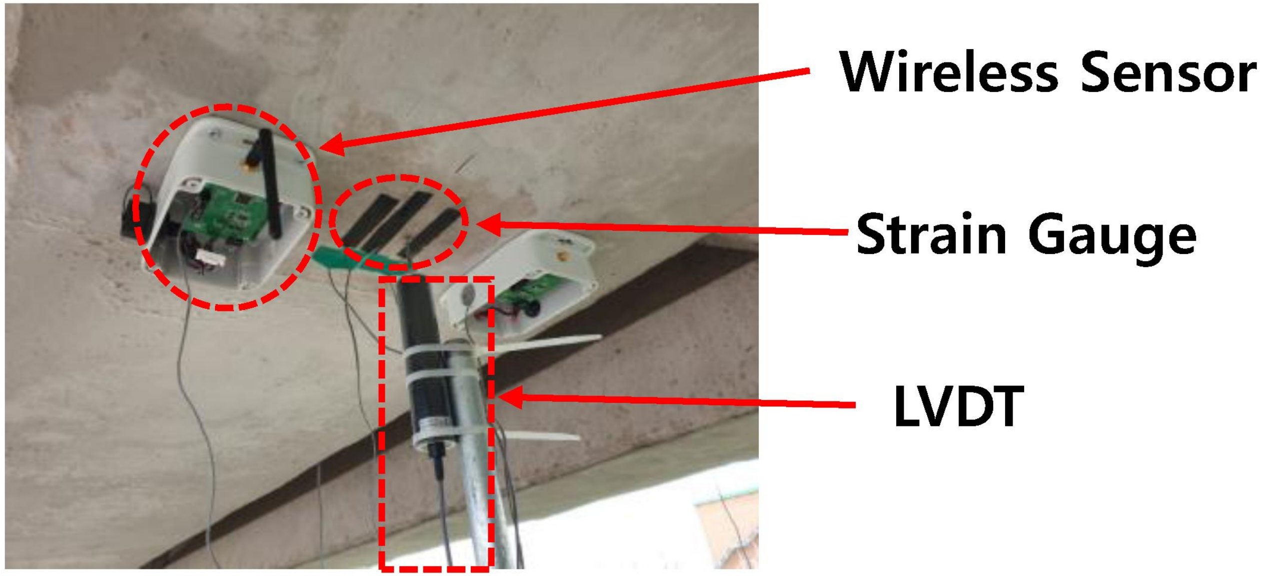

5.1 Research Background

In contrast, vision-based measurement provides non-contact, full-field vibration monitoring, delivering comprehensive data for bridge displacement analysis.

The model can be placed on a vibration table for high-frequency simulations. Ordinary cameras can't meet the required frame rates, so we use high-speed cameras to monitor and analyze the model. This ensures accurate data collection for detailed research, crucial for understanding dynamic behavior.

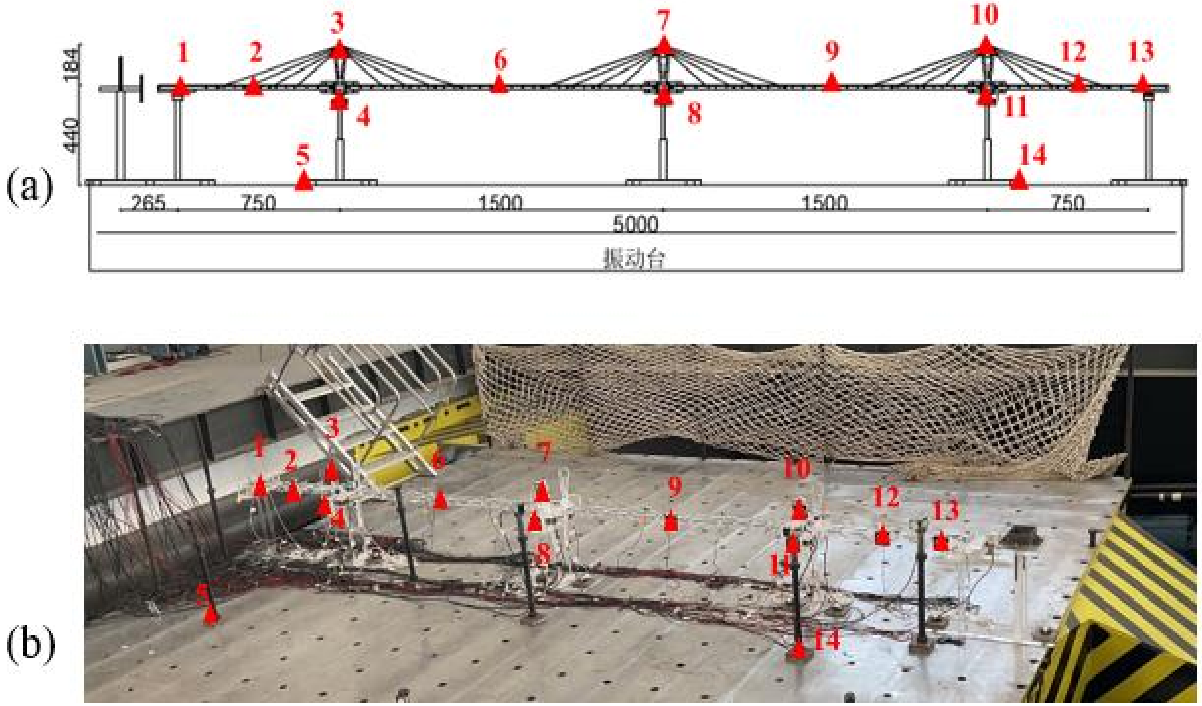

Monitoring Points for Cable-Stayed Bridge Structures

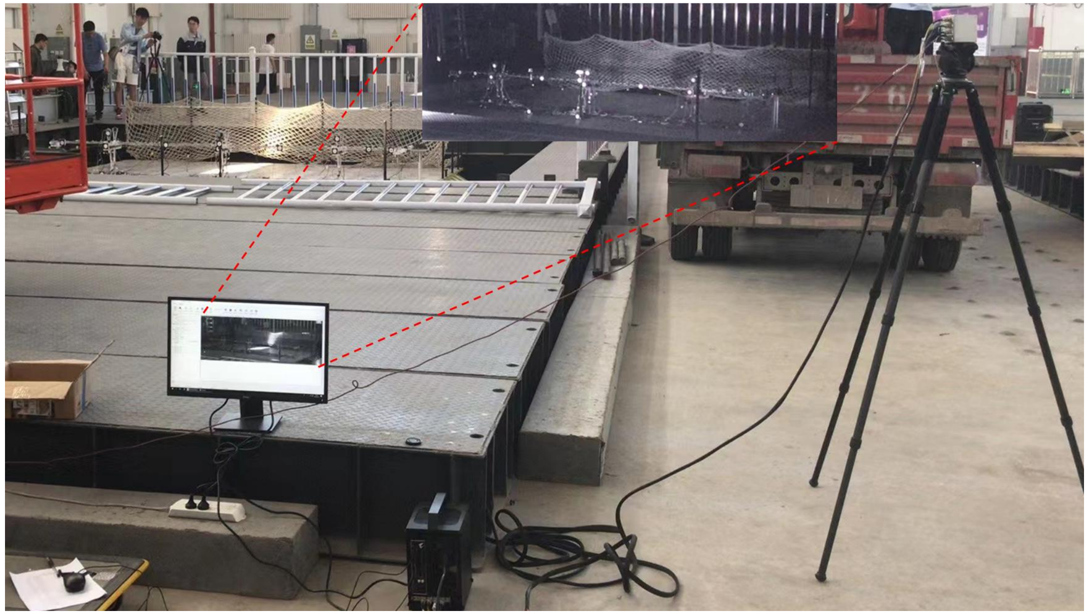

Experimental Setup

5.2 High-Speed Camera System

Professional photography equipment has a maximum frame rate of 240 frames per second, which makes it difficult to accurately capture high-speed moving objects encountered in daily life and scientific research. There is a need for industrial high-speed cameras with higher frame rates and resolutions.

	**Japan Photron FASTCAM Nova R5** Video shooting capability: 4096x2304 (9.4 million pixels) 1250 fps 1920x1080 (1.3 million pixels) 5280 fps
	**USA Phantom TMX 7510** Video shooting capability: 1280x800 (1 million pixels) 7.5 million fps 640x128 (80,000 pixels) 87.5 million fps

5.2 High-speed Video Measurement

Three-dimensional (3D) stereoscopic measurements, by leveraging the principles of stereoscopy, offer the remarkable possibility of extracting detailed three-dimensional spatial information from a pair of two-dimensional (2D) images.

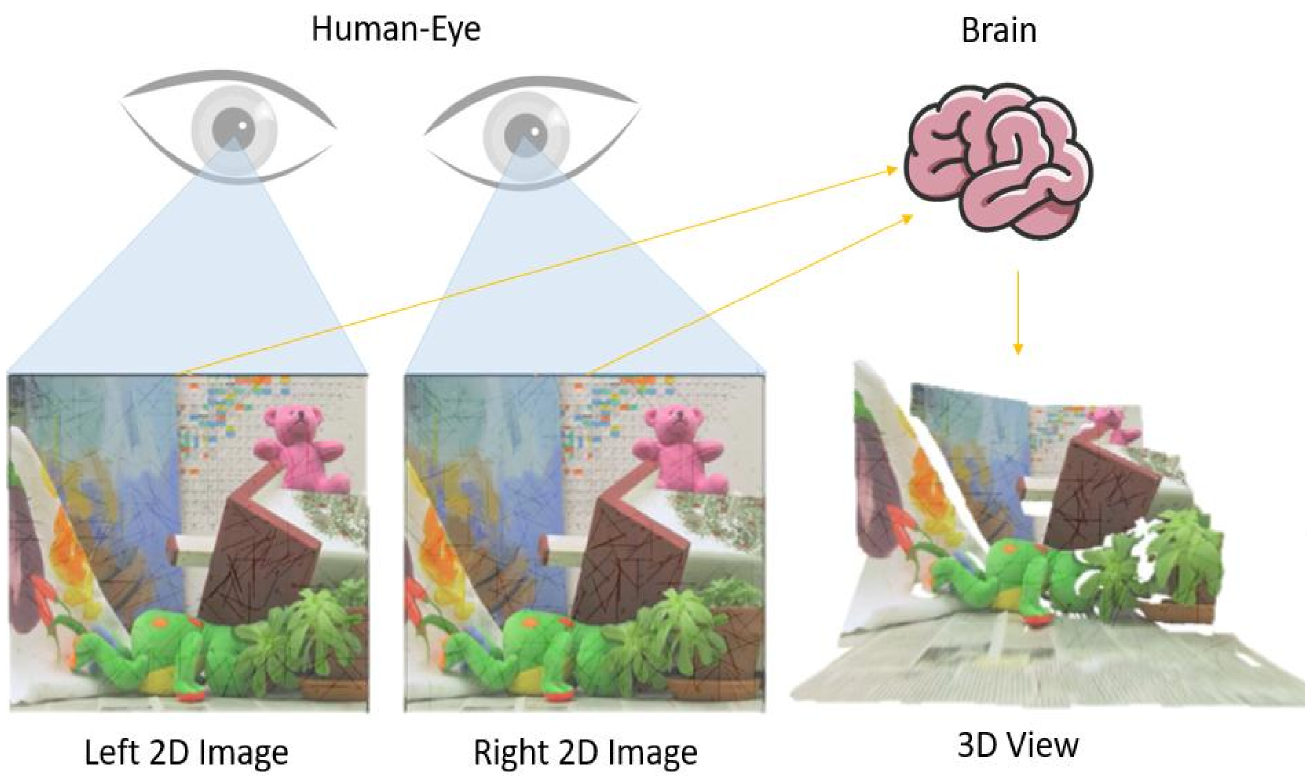

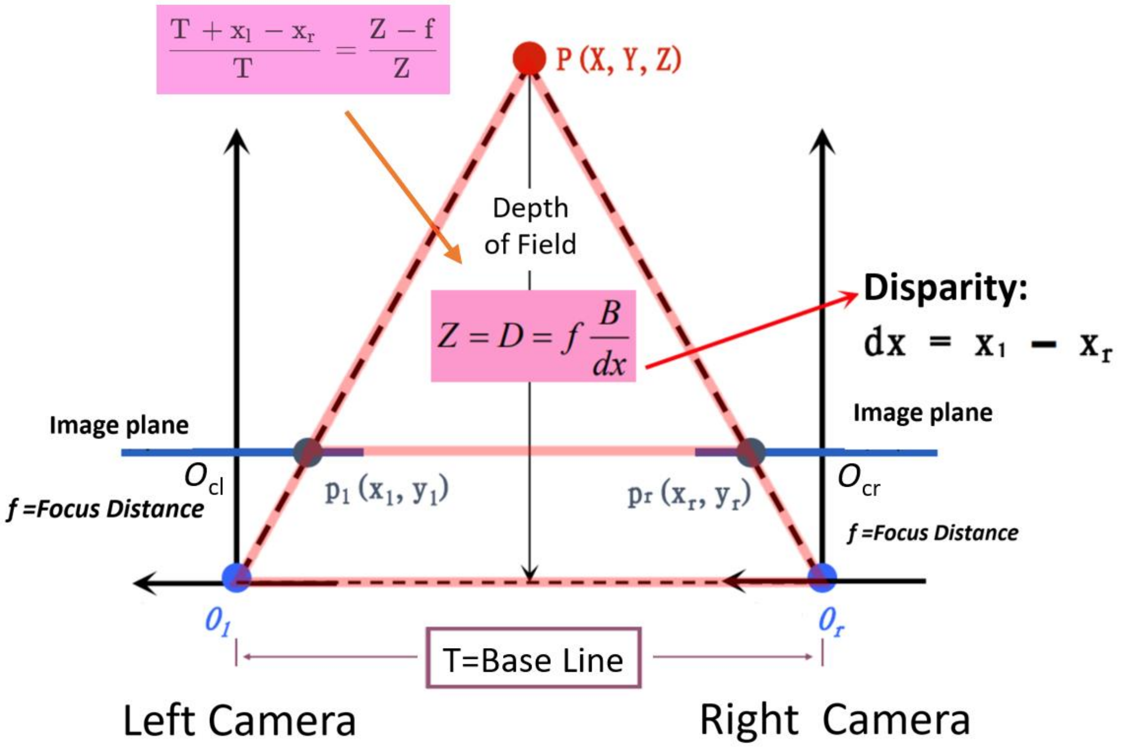

5.3 High-Speed Camera System

Traditional planar measurement employs a single camera for image acquisition with internal storage, featuring a relatively simple structure. In contrast, high-speed stereoscopic measurement utilizes multiple synchronized cameras to derive spatial coordinates through geometric relationships, requiring a more sophisticated industrial high-speed camera system.

Common Digital Camera

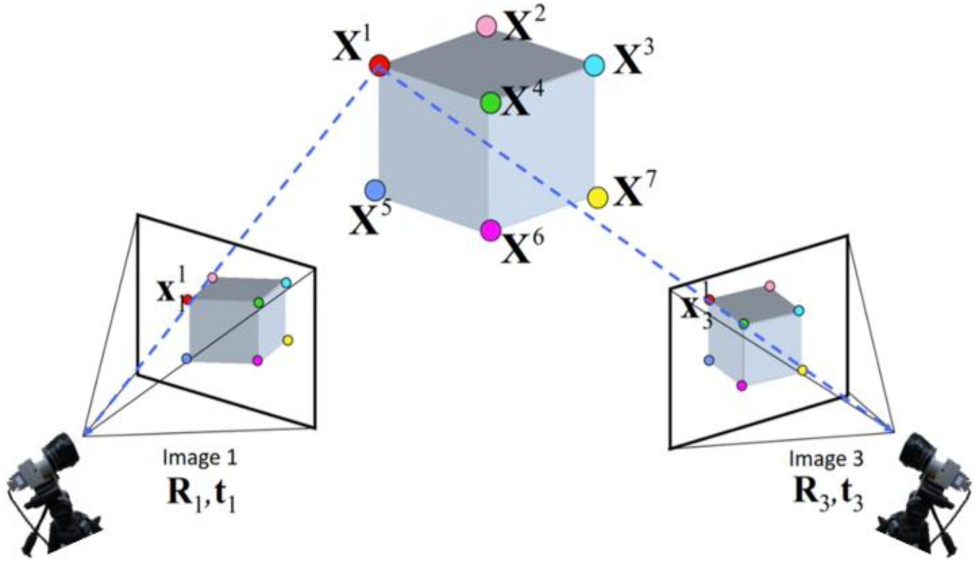

stereo measurement

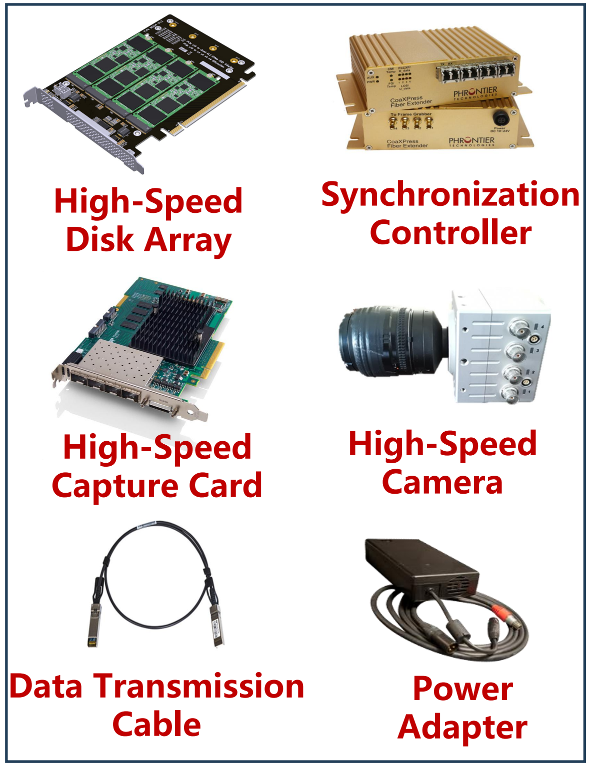

High-Speed Camera System

5.3 High-Speed Camera System

Multi-node Cooperative Distributed Networking

A distributed networking real-time processing technology with multi-node collaboration is proposed to solve the problems of easy overloading of centralized storage and low efficiency of data solving, and to efficiently realize image capturing, storage and control.

Level 1 Node
High Speed Camera
->Image Capture

Level 2 Node
Industrial Control Computer
->image storage

Level 3 Node
Sync Trigger
->Frame Synchronization

Level 4 Node
Master Control Computer
->Image Acquisition Control

5.4 Image Sequence Processing

Camera calibration is necessary due to lens distortion and the need for intrinsic and extrinsic parameters in 3D reconstruction. Using calibration objects with known geometry, these parameters are obtained to accurately convert 2D image coordinates to 3D spatial coordinates, ensuring precise measurements and reconstruction.

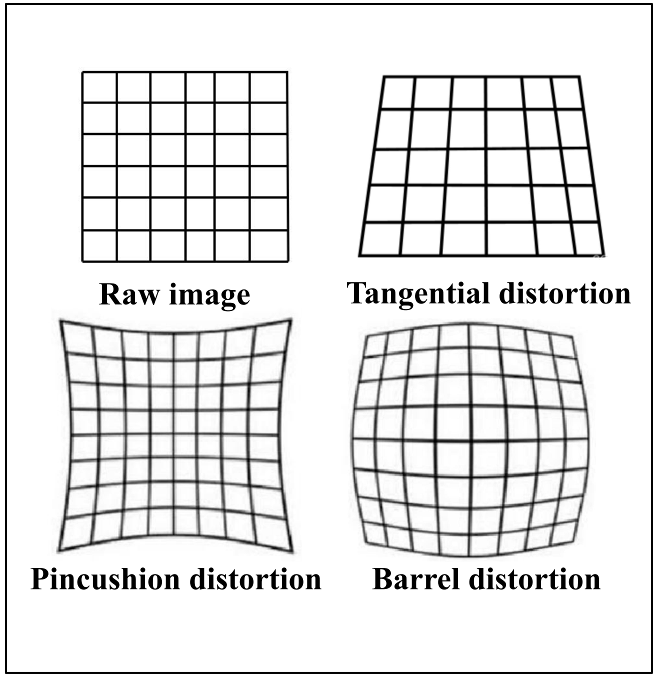

Camera intrinsic parameters

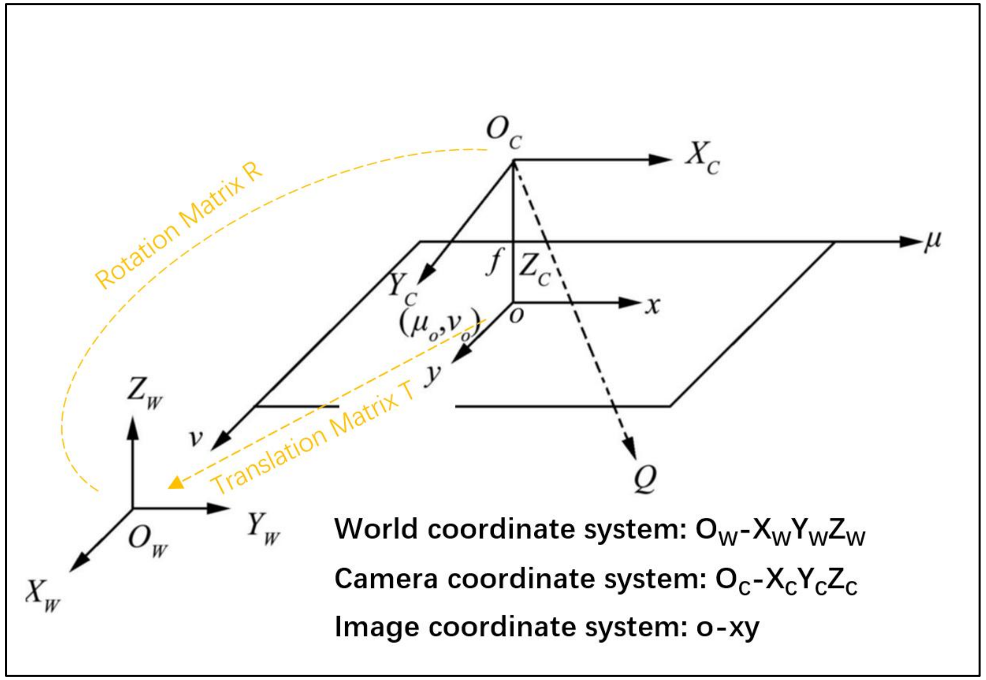

Camera extrinsic parameters

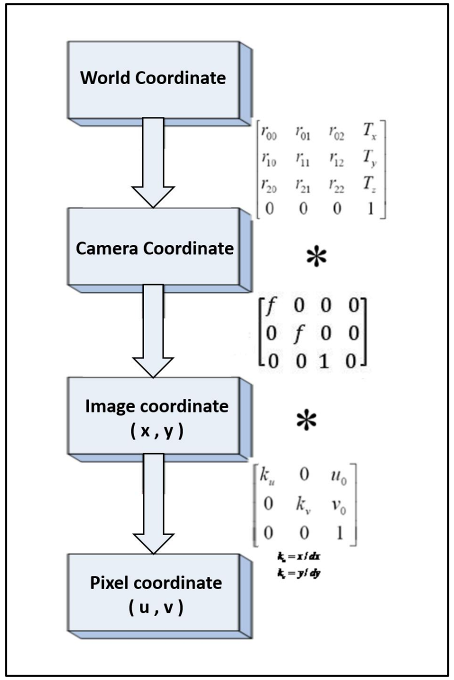

Coordinate transformation

5.4 Image Sequence Processing

Accurate target point recognition is key to obtaining object motion data, often using markers like ellipses on the object. Recognition involves edge detection and morphological operations to extract features, followed by elliptical fitting for precise positioning. Tracking these points captures position changes, analyzing trajectory, velocity, and acceleration while maintaining high precision despite occlusions or environmental changes.

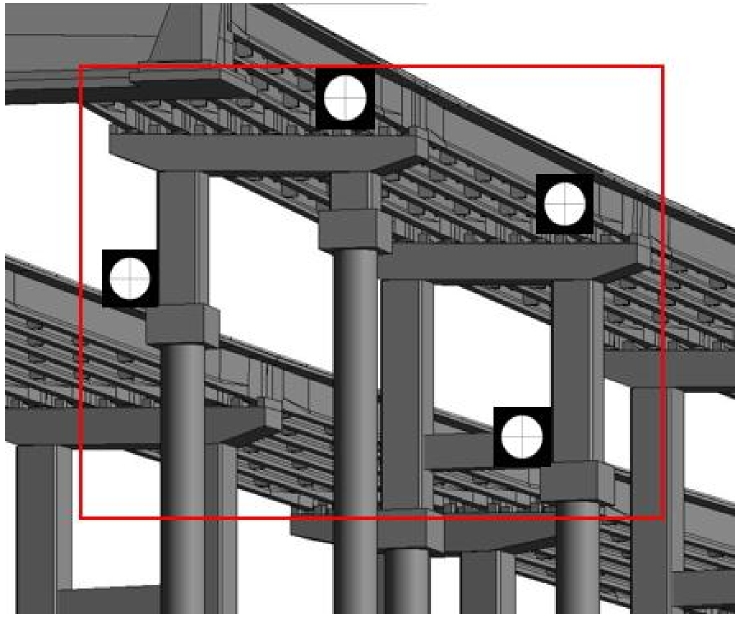

Marker Placement

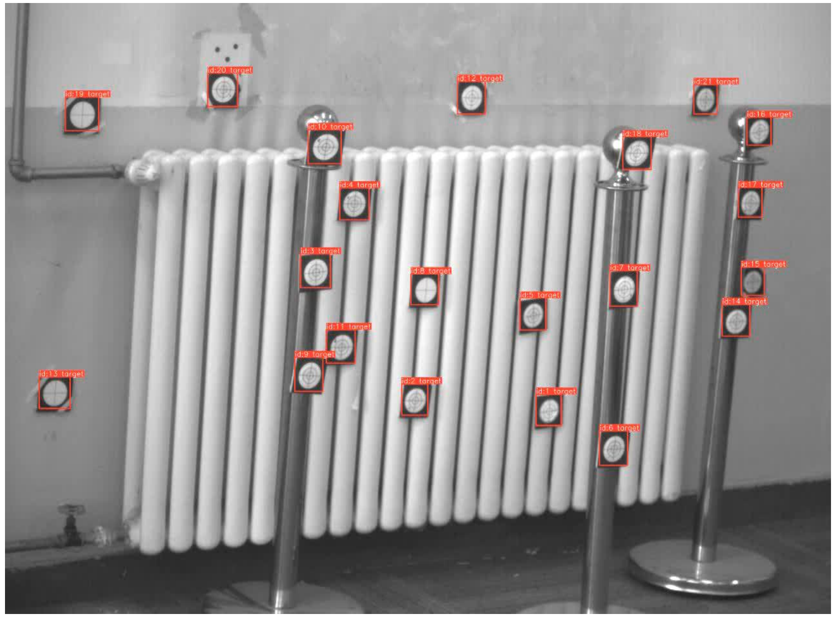

Target point tracking

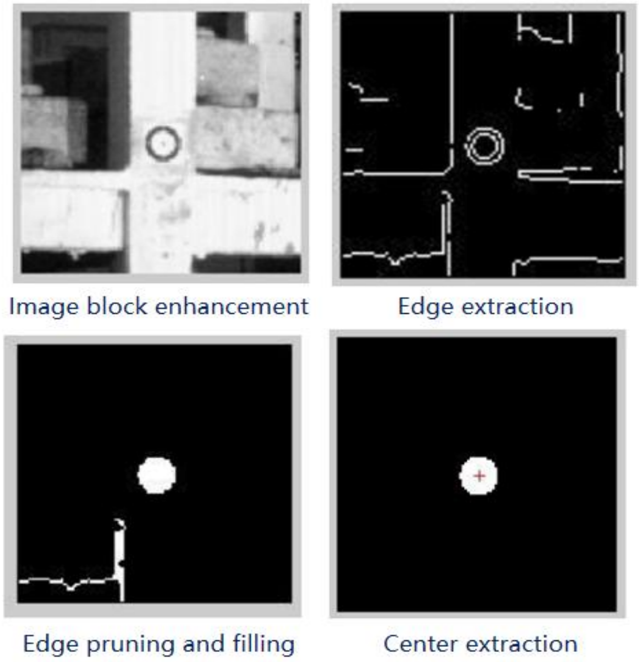

Identification and tracking

5.4 Image Sequence Processing

To achieve the extraction of three-dimensional information from two-dimensional images, it is necessary to identify representative image points for disparity calculation.

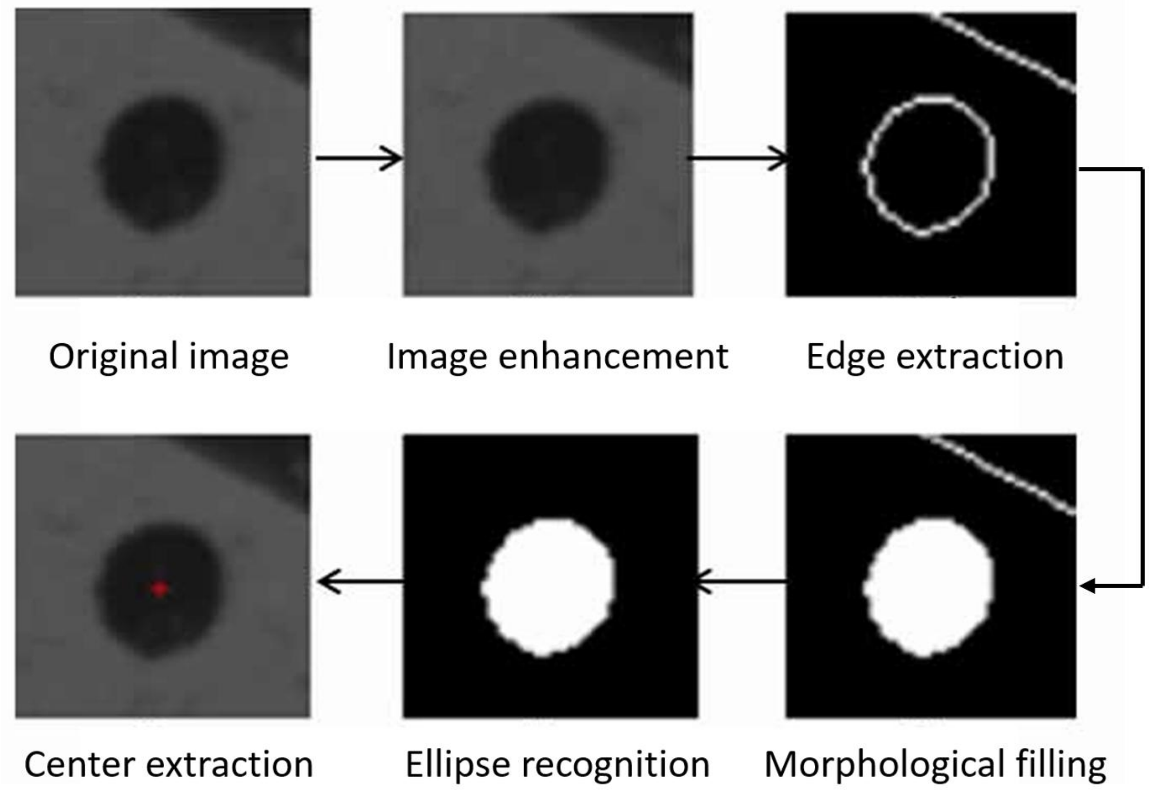

Target Point Extraction

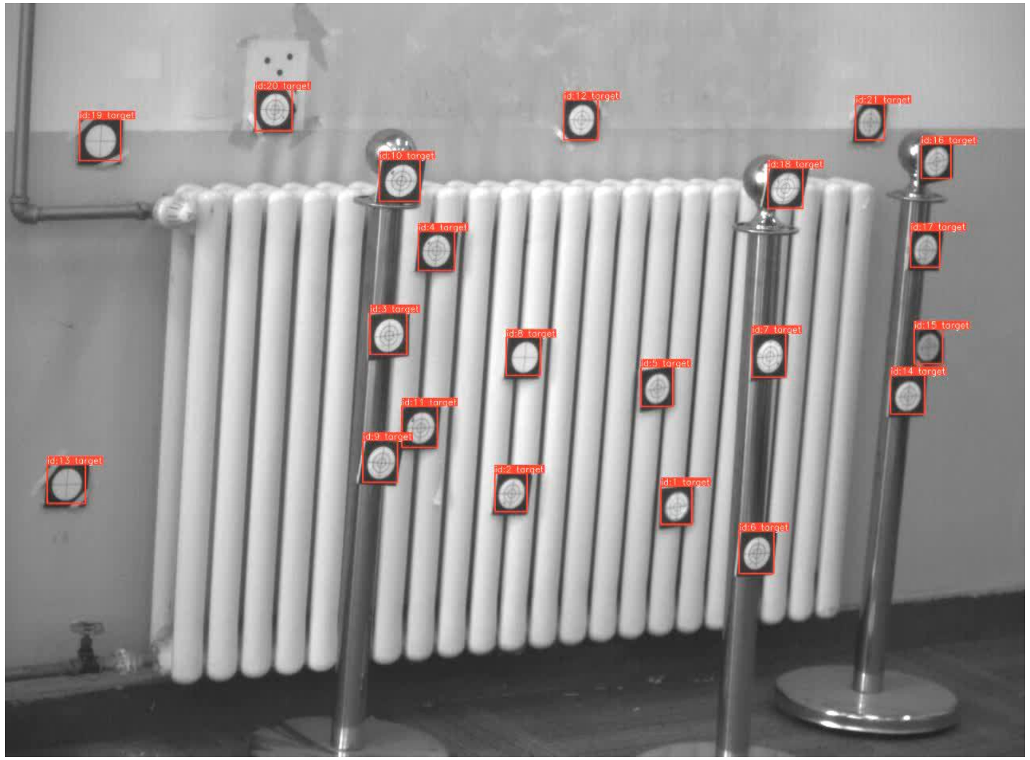

Target Point Match

5.4 Image Sequence Processing

Matching identifies feature point correspondences across frames or viewpoints, crucial for 3D reconstruction. Methods include SIFT, SURF, optical flow, template matching, and phase correlation. The goal is to obtain the 3D displacement curve, reflecting the object's position changes over time, supporting mechanical analysis and behavior simulation.

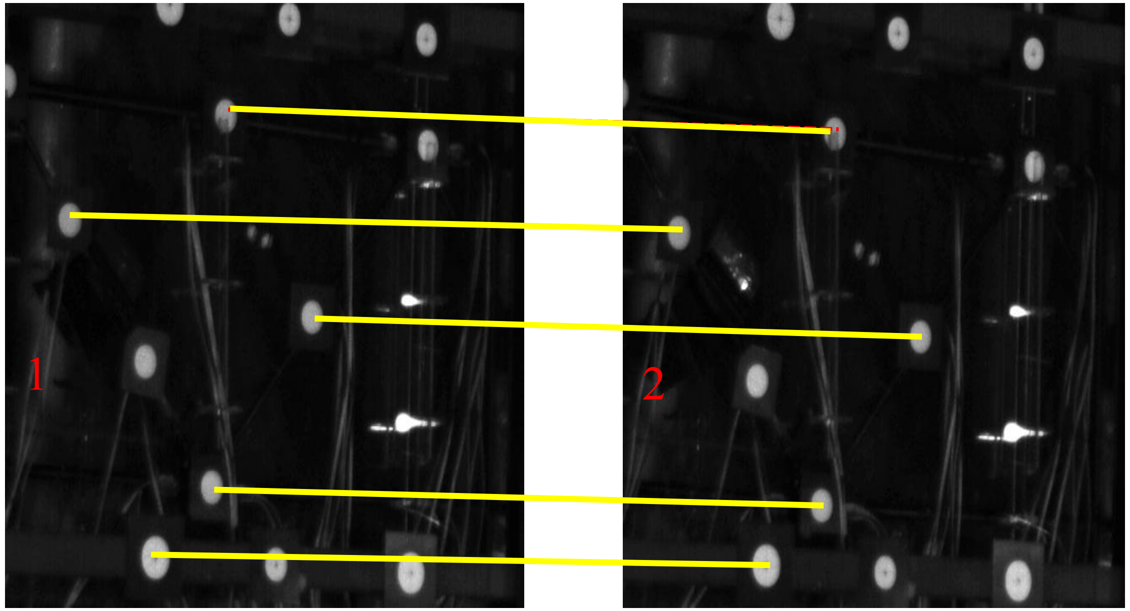

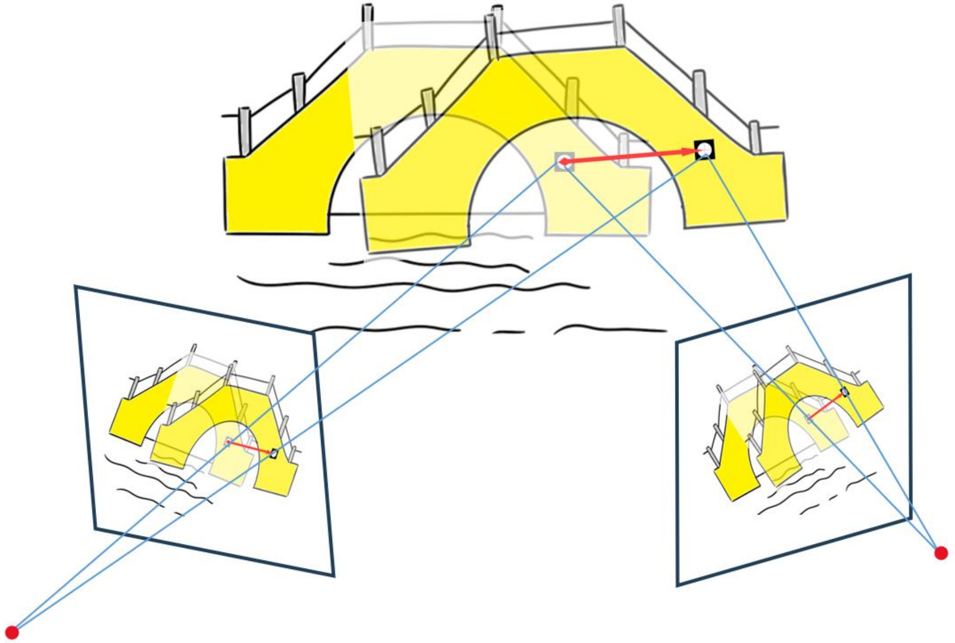

Feature Point Matching

Catalogue

6 Conclusion

Multi-source remote sensing monitoring technology has been initially applied in Beijing, China. It will be used by a wider space for urban infrastructure monitoring in the future.